Chapter 13
Modelling in Membrane Separation of Bioactives

Krishnasri V. Kurada, Sourav Mondal, and Sirshendu De

Abstract Membrane based systems have become integral parts of the processing of bioactive compounds from the plant extract or fruit/vegetable juice. The technical feasibility of the process is generally established experimentally in small scale laboratory set ups. The results in the lab scale experimental data are generally used to scale up the process to the industrial level. To achieve this, a suitable model is needed. The major aspects of modelling the membrane-based systems are the prediction of the permeate flux and permeate concentration of the target species. These two parameters are related to the process throughput and quality of the product stream. The actual extract or juice is a complex fluid with an assortment of various components. Therefore, it is quite difficult to estimate the physico-chemical and transport properties of the extract/juice making the formulation of a physical model almost untenable. In this context, the popular models for tracing the behavior of the membrane-based systems are classified into three categories, namely, empirical, semi-empirical and transport phenomena based models from first principles. These three classes of the models are discussed in depth in this book chapter in relevance to the processing of the bioactive components. The assumptions, underlying physical principles, advantages, limitations and applicability of various models are discussed with great details. The models are also demonstrated with the practical case studies. It is envisaged that the presentation in this chapter would be of immense help to the design engineers to model and subsequent scaling up of the membrane processing of the production of bioactive components from the plant extract or the fruit/vegetable juices.

Keywords Bio-actives · Membranes · Modelling · Permeate flux · Fouling · Scale-up

K. V. Kurada · S. Mondal · S. De (✉)
Department of Chemical Engineering, Indian Institute of Technology Kharagpur, Kharagpur, India
e-mail: sde@che.iitkgp.ac.in

Nomenclature

A_m	Effective area of the membrane (m^2)
a and b	Pressure dependency parameters of mass transfer coefficient
B_1	Phenomenological membrane transport coefficients of permeation (m^3/m^2.s)
C_{0i}	Initial concentration of ith component (kg/m^3)
C_{ib}	Bulk concentration of ith component (kg/m^3)
C_{ig}	Concentration of ith component in gel layer (kg/m^3)
C_{pi}	Permeate concentration of ith component (kg/m^3)
d_e	Effective diameter of the channel (μm)
D_i	Diffusivity of ith component (m^2/s)
G_1 and G_2	Dimensionless parameters
J	Permeate flux (m^3/m^2 s)
J_0	Permeate flux at $t = 0$ (m^3/m^2 s)
J_w	Permeate flux using pure distilled water (m^3/m^2 s)
k and n	System specific parameters of Hermia's model
k' and m	System specific parameters of Field's model
k_1	Complete pore blocking constant
k_2	Intermediate pore blocking constant
k_c	Cake filtration constant
k_f	Mass transfer coefficient (m/s)
k_{f1}	Pressure dependent mass transfer coefficient
k_g	The parameter responsible for the rapid or slow growth of the fouling layer
L	Gel layer thickness (μm)
M_w	Molecular weight (kDa)
N	No. of experiments
n_1	Exponent in the pressure dependency expression of ε and α
ΔP	Transmembrane pressure drop (kPa)
Q	Volumetric flow rate (m^3/s)
R_{bl}	Resistance due to boundary layer (m^{-1})
R_F	Fouling layer resistance (m^{-1})
R_g	Gel layer resistance (m^{-1})
R_m	Membrane hydraulic resistance (m^{-1})
R_p	Pore blocking resistance (m^{-1})
Rr	Real retention
R_T	Total resistance (m^{-1})
S_0 and S	Square of errors
T	Temperature (K)
t	Time (s)
t_{PB}	The time up to which the pore blocking prevails (s)
u	Cross flow velocity (m/s)
V	Volume (m^3)

| v_1, v_2 and v_3 | Dimensionless parameters |
| w | Width of the filtration cell (cm) |

Greek Letters

α	Specific gel resistance (m/kg)
α_0	Pressure independent specific gel resistance (m/kg)
β	Gel layer resistance per unit length (m^{-1} kg^{-1})
δ	Thickness of the concentration boundary layer (µm)
ε_g	Porosity of the gel layer
ε_0	Pressure independent porosity of the gel layer
γ_g	Partition coefficient
ϕ	Standard pore blocking constant
μ	Viscosity of the permeating solution (kg/m s)
μ_w	Viscosity of water (kg/m s)
π	Osmotic pressure (kPa)
ρ_g	Density of the gel layer (kg/m^3)
ρ_f	Density of the feed stream (kg/m^3)
ρ_p	Density of the permeate stream (kg/m^3)
σ_1	Phenomenological membrane transport coefficients of reflection
τ	Non-dimensional parameter

Abbreviations

CFR	Cross flow rate
EGCG	Epigallochatechin gallate
HMW	High molecular weight
LMW	Low molecular weight
MWCO	Molecular weight cut-off
PSf	Polysulfone
TMP	Transmembrane pressure drop
TDS	Total dissolved solids

1   Introduction

Extraction of bioactive compounds from plant extracts is a sequential process of five distinct stages, namely, (1) pre-treatment, (2) separation of macro and micro- nutrients, (3) extraction, (4) isolation-purification and finally (5) product formation or encapsulation (Galanakis 2015). Pre-treatment of the feed is an important step to

separate the large molecular weight compounds and is being carried out using either microfiltration (MF) or ultrafiltration (UF) membranes (Galanakis 2015; Kumar et al. 2012). Also, removal of microbes is an important step to be ensured during the processing of bioactives. However, majority of microbes are generally removed by 0.2 μm MF membranes and all of them are excluded by lower sized UF membranes. Currently, membrane based processes have become an integral unit operation for treatment of liquid streams of widely varying composition in chemical, food, biotechnology and pharmaceutical industries (Pabby et al. 2015). Membrane filtration finds diverse applications in separation and fractionation of bioactives, concentration of fruit juices, removal of coagulating proteins, fibrous substances and microorganisms. Such specialized filtration is pertinent for the extraction of bioactive compounds from plant extract because (1) the membrane processing can be done under room temperature precluding denaturation at higher temperature; (2) no chemicals are needed during separation and (3) microorganism can be removed easily in single step (Gerke et al. 2017; Mondal and De 2018). Although, the membranes are capable of separating compounds via sieving mechanism based on their molecular size, their selectivity can be tuned by exploiting the operating conditions and various membrane modification techniques thereby expanding their applications in the food industry over the last few years.

Application of membranes filtration for processing plant extracts or fruit juices for selective separation of various nutrients or specific compounds having pharmaceutical applications has been investigated extensively. Several researchers have studied the performance of membrane based separation processes for filtration of various fruit juices, e.g., apple, pomegranate, grape, orange, watermelon, kiwi etc., (Aghdam et al. 2015; Cancino-Madariaga et al. 2012; Conidi et al. 2012; Giacobbo et al. 2017; Mondal et al. 2011; Rai et al. 2010; Vladisavljević et al. 2003). The application of membranes to extract specific bioactive compounds from various plant extracts has been also attempted. For example, ultrafiltration membranes were used to enrich the important phytochemicals, such as epigallochatechin gallate (EGCG) from aqueous extract of green tea leaves (Kumar et al. 2012; Mondal and De 2018) Mondal and De 2019; dos Santa Sousa et al. 2016). Extraction of Stevioside from the extract of Stevia leaves using membrane filtration has been extensively studied owing to its high antioxidant, anti-carcinogenic and anti-diabetic properties (Das et al. 2015; Mondal et al. 2012a, b, 2013; Reis et al. 2009; Roy and De 2014, 2015). Rai et al. have used microfiltration membranes to separate nutrients like lycopene from watermelon extract (Rai et al. 2010). Few researchers have attempted selective separation of bioactive peptides from protein hydrolysate using membrane filtration (Agyei and Danquah 2011; Firdaous et al. 2009; Poulin et al. 2006).

The major drawback of the membrane separation process is the decrease in permeate flux due to the membrane fouling (Ilame and Satyavir 2015; Mondal et al. 2013; Roy and De 2015). Fouling of the membrane cannot be avoided but they can be minimized. Various techniques are used to reduce the membrane fouling. These are: (1) modification of the membrane surface by making it more hydrophilic and smooth, incorporating antifouling additives, surfactant treatment, etc. (Kurada and De 2018; Mukherjee and De 2016; Song et al. 2000); (2) altering the

hydrodynamics in the flow channel by increasing the turbulence, creating Dean vortices, use of turbulent promoters, etc. (Guo et al. 2012; Jaffrin 2012; Ma et al. 2000); (3) use of external fields, like, electric and magnetic (Jian et al. 2006; Wandera et al. 2010). Therefore, modelling of membrane filtration to quantify the flux decline a-priori is of paramount importance to have an efficient design of the process and also to estimate the membrane life.

The models of the membrane flux decline can be categorized into the following groups, namely, (1) empirical models, like, resistance in series models; (2) semi-empirical models, like, blocking models; (3) transport phenomena based models using first principles to quantify the underlying physics of the system. The resistance-in-series models are entirely empirical in nature and various transport resistances are estimated from the experimental permeate flux data. Since, the correlations are developed over a range of operating conditions, such models are valid within that range only and they lose their predictability beyond those. Although the semi-empirical blocking models (different models are proposed for various fouling mechanisms) are based on the theoretical background of the filtration mechanisms, the flux decline is expressed in terms of the filtration coefficient that is estimated by optimizing the experimental flux decline profile. The fouling mechanism is identified by testing the closeness of fitting the experimental flux decline data to the calculated ones, indicated by correlation coefficient between the experimental and calculated datasets. In majority of the cases, the correlations coefficients are too close to attain a definite conclusion about the flux decline mechanism. Additionally, both resistance-in-series model and blocking model can quantify the permeate flux, not the bioactive concentration in the permeate. Therefore, these models cannot account for the recovery and selectivity of the bioactive compounds in the filtrate. On the other hand, the transport phenomena-based models are derived from the first principles and they can estimate both the permeate flux and permeate quality as a function of time. The aqueous solution of a plant extract being a complex fluid having a large number of solutes with varying concentration, the transport coefficients, such as solute diffusivity, membrane permeation coefficient, etc., are estimated using the experimental data, imparting a semi-empirical flavour to such models. However, once the parameters are estimated from a selected experimental data, such model can be used for other operating conditions, scaling up calculations in completely predictive mode for the same plant product and bioactive component. Thus, the third category of the models is versatile having wider applicability and broader predictive capability.

The present chapter focuses on the critical challenges involved in the modelling of the membrane-based processes for extraction of bioactive molecules. The details of various fouling models as described above, their solution and applications are discussed. Given a model, the optimization procedure to select the operating conditions is also presented. The modelling aspects of the permeate flux hysteresis observed during ultrafiltration of plant extract is also addressed. It is envisaged that this chapter would be of immense help to the design engineers to adopt an appropriate model and design the membrane-based filtration for bioactive compounds efficiently.

2   Modelling Aspects of Membrane-Based Separation

The major drawback of membrane separation processes is the decrease in permeate flux i.e., throughput of the process, as well as the quality of permeate due to membrane fouling (De et al. 1997). Fouling of membrane takes place due to the blocking of pores by the solute particles or by the deposition of the solute particles over the membrane surface resulting into increase in osmotic pressure across the membrane surface (Bungay et al. 1983). Fouling is mainly of two types, reversible and irreversible (Mondal et al. 2012b). When membrane permeability can be regained after appropriate washing, it is termed as reversible fouling. On the other hand, irreversible fouling cannot be eliminated completely and corresponds to partial gain in the membrane permeability (Mondal et al. 2012b). The main contributing factor of reversible fouling is the accumulation of solute particles on the membrane surface also known as concentration polarization (De et al. 1997). Permeate flux throughput and product quality are two important parameters to be predicted for efficient design and subsequent scaling up. Following sections discuss different approaches used for modelling of membrane-based process used for separation of bioactive compounds.

2.1   Empirical Models

The operating parameters play an important role on the performance and life of the membrane during separation of complex solutions (Padaki et al. 2015). In this regard, a simple model for quantification of permeate flux decline is very useful. Identification of phase space of operating parameters for optimal performance of the filtration process can be an effective tool for easy scale up and design. Few authors have attempted quantification of flux decline for real life, complicated streams (Mondal and De 2018; Mondal et al. 2011; Rai et al. 2010; Roy and De 2015). Roy and De have used resistance in series model to optimize the operating conditions for filtration of Stevial glycoside extracts using ultrafiltration (Roy and De 2015). Mondal et al., have formulated the resistance in series model to model the flux decline during microfiltration of fresh green tea extract (Mondal and De 2018). Tasselli et al., have analysed the permeate flux decline of ultrafiltration of kiwi fruit juice in terms of this model (Tasselli et al. 2007). Several other authors have quantified the flux decline during membrane filtration of fruit juices and bioactive compounds using this model (Skinner and Hunter 2013; Vladisavljević et al. 2003). Therefore, the advantage of this model is the easy design and scaling up as already discussed. However, the limitations of the model are, (1) the permeate flux can only be quantified as a function of time but not the permeate concentration; (2) the model is specific to the system considered due to the empiricism involved in the model; (3) the model parameters are valid within the studied range of operating parameters. Thus, the resistance-in-series models are neither to be considered as predictive tools

to quantify the flux decline, nor they are generalized enough to be applicable for different juices/ extract, thereby losing their versatility.

2.1.1   Resistance in Series Model

Usually the plant extract is a complex mixture containing a large number of solutes with varying molecular weight and concentration. Therefore, it is difficult to identify each of them with their respective concentration. Moreover, their transport properties, such as diffusivity, intrinsic membrane rejection, solution osmotic pressure, etc., are not accurately known. For this reason, the resistance in series model becomes quite easy and handy for the description of the permeate flux decline. In this model, various resistances against the permeate flux are considered to be acting in series (with the analogy of electric circuit) and the permeate flux is quantified as the driving force (transmembrane pressure drop in this case) divided by the total resistance. One or more of these resistances may be function of time. The resistances are estimated from the experimental permeate flux decline data and their functional variation with time is correlated with the operating conditions, like, transmembrane pressure drop (TMP) and cross flow rate (CFR). This provides the utility of this model to interpolate the flux decline with the unknown operating conditions.

Various resistances encountered by the permeate flux are: membrane hydraulic resistance (R_m), fouling layer resistance (R_F) and pore blocking resistance (R_p). The membrane hydraulic resistance (R_m) is calculated using (Gerke et al. 2017) as:

$$R_m = \frac{\Delta P}{\mu_w J_w} \tag{13.1}$$

where, ΔP is the transmembrane pressure drop (TMP), μ_w is the viscosity of water and J_w is the permeate flux using pure distilled water (having no osmotic pressure). For some solutes, pore blocking resistance is absent, if the solute size is much larger than the membrane pore size. In such cases, pore blocking resistance can be neglected and the fouling layer resistance, R_F can be represented in terms of the experimental permeate flux as (Mondal and De 2018):

$$R_F = \frac{\Delta P}{\mu J(t)} - R_m \tag{13.2}$$

In above equation, μ is the viscosity of the permeating solution and $J(t)$ is the permeate flux at any time point t when the plant extract/juice is used as the feed solution. It may be mentioned that the fouling resistance is mostly reversible in nature in absence of membrane pore blocking.

In case of the presence of significant pore blocking resistance (R_p), it is estimated in two ways. In the first case, the irreversible resistance of the membrane during N^{th}

experiment is estimated by measuring the pure water flux before and after the experiment. This resistance is a measure of irreversible membrane resistance even after membrane cleaning (Roy and De 2015).

$$R_P^N = \frac{\Delta P}{\mu_w J_w^{N-1}} - \frac{\Delta P}{\mu_w J_w^N} \tag{13.3}$$

In the above equation, R_P^N is the pore blocking resistance during N^{th} experiment, J_w^{N-1} is the pure water flux after N-1th (i.e., the water flux before starting the Nth experiment) and J_w^N is the pure water flux after N^{th} experiment using the cleaned membrane. Thus, R_P^N is an indicator of the resistance corresponding to irreversible membrane fouling during N^{th} experiment. In such cases, the fouling resistance cannot be determined a straightforward way like the case without pore blocking resistance. Here, the fouling resistance at any time of filtration is estimated from the experimental permeate flux data as:

$$R_F = \frac{\Delta P}{\mu J(t)} - R_m - R_P^{N-1} \tag{13.4a}$$

where, $J(t)$ is the permeate flux at any time point t. The modelling aspects of these two cases are discussed in detail as follows.

In the second case, the pore blocking resistance during the filtration is measured by observing the nature of the flux decline. If the initial (short term) flux decline is rapid, it envisaged that some of the membrane pores are getting blocked completely or partially leading to rapid flux decline. The flux decline becomes gradual thereafter (long term) due to deposition of solute particles over the fouling layer. The short-term flux decline due to pore blocking is quantified as:

$$R_P = \frac{\Delta P}{\mu J(t)} - R_M \tag{13.4b}$$

The above equation is valid for $0 < t < t_{PB}$, where, t_{PB} is the time up to which the pore blocking prevails (time point at the end of rapid flux decline or the end of short term flux decline; this time point is identified for the experimental permeate flux decline data).

Resistance in Series Model Without Pore Blocking

For an industry relevant cross flow system, the growth of the fouling layer attains a steady value due to the arresting of the growth of the fouling layer over the membrane surface by the forced convection imposed by the cross-flow rate. Thus, the rate of increase of fouling resistance at any time point is proportional to the

difference between the fouling resistance at steady state and fouling resistance at that instance (De et al. 1997; Mondal and De 2018), as follows:

$$\frac{dR_F}{dt} \propto \left(R_F^S - R_F\right) \tag{13.5}$$

where, superscript s stands for steady state. The above expression, integrated with the initial condition, at $t = 0$, $R_F = 0$ results into:

$$R_F = R_F^S \left[1 - \exp\left(-k_g t\right)\right] \tag{13.6}$$

In the above expression, k_g is the constant of proportionality representing the parameter responsible for the rapid or slow growth of the fouling layer. Larger value of k_g indicates faster growth rate of the fouling layer. A plot of $\ln\left[\dfrac{R_F^S}{R_F^S - R_F}\right]$ against

't' indicates a straight line passing through the origin and the slope of this line gives the value of k_g. The fouling resistance at the steady state (R_F^S) is estimated from Eq. (13.2), by replacing $J(t)$ by $J^s(t)$, the steady state permeate flux. The steady state permeate flux is a strong function of the operating parameters, TMP and CFR. In general, the permeate flux increases with TMP stronger at its lower range and the increase is sluggish at higher TMP. The permeate flux is typically an increasing function of cross flow rate due to higher Reynolds number (Re). On the other hand, k_g is mostly a characteristic of the solution (fruit juice or plant extract) and varies weakly with the operating conditions. R_m is measured from the permeability of the membrane using Eq. (13.1) and remains constant for all experiments. Thus, the time variation of the permeate flux (J) can be estimated by using the calculated values of k_g and the estimated values of R_m and R_F^S at the operating TMP using the following equation (Mondal and De 2018):

$$J(t) = \frac{\Delta P}{\mu \left[R_m + \left\{R_F^S \left(1 - \exp(-k_g t)\right)\right\}\right]} \tag{13.7}$$

As discussed above, the steady-state fouling resistance is a function of different operating conditions and can be expressed in terms of TMP and Reynolds number. This model was used by Mondal and De to quantify the flux decline during the microfiltration of green tea extract with an aim to enrich the bioactive compound EGCG (Mondal and De 2018). The experiments were conducted in hollow fiber configuration and the variation TMP in that study was in the range of 35 to 172 kPa and that of Re was from 94 to 282. The functional variation of the steady-state fouling resistance was described through a correlation using the experimental data as (Mondal and De 2018):

$$\frac{R_F^S}{R_M} = \left(0.34 - 2.72 \times 10^{-4}\,\text{Re}\right)\exp\left(1.148 \times 10^{-4}\,\Delta P\right) \tag{13.8}$$

The values of k_g were estimated as described earlier and found to vary in a narrow range 0.001 and 0.0017 s^{-1} and an average value of 0.0015 s^{-1} was considered. Thus, the overall design equation of permeate flux at a given instant for any operating condition was presented as (Mondal and De 2018):

$$J(t) = \frac{3.6 \times 10^6\,\Delta P}{\mu R_m \left[\begin{array}{c} 1 + \left(0.34 - 2.72 \times 10^{-4}\,\text{Re}\right)\exp\left(1.148 \times 10^{-5}\,\Delta P\right) \\ \times \left\{1 - \exp\left(-0.0015t\right)\right\} \end{array} \right]} \tag{13.9}$$

The permeate flux at the steady state (J^s) can be obtained from Eq. (13.9) by substituting $t \to \infty$. The limiting permeate was therefore determined using Eq. (13.9) by equating $\frac{dJ^s}{d\varnothing P}$ to zero. The resultant equation provides a trajectory of ΔP and Re so that the limiting steady state permeate flux (limiting flux is defined as the flux that does not increase beyond a particular ΔP, termed as ΔP_{lim}) can be achieved (Bacchin et al. 2006; Field and Pearce 2011; Mondal and De 2018). Thus, the interrelation of ΔP_{lim} and Re for such limiting flux condition was:

$$\left[1.148 \times 10^{-5}\,\Delta P_{\text{lim}} - 1\right]\exp\left(1.148 \times 10^{-5}\,\Delta P_{\text{lim}}\right) = \frac{1}{0.34 - 2.72 \times 10^{-4}\,\text{Re}} \tag{13.10}$$

The above relation provides a combination of TMP and Re that provides the limiting permeate flux. Using the above equation one can select a TMP at a particular Re number so that the maximum (limiting) permeate flux is obtained. At this point, the concept of threshold TMP may also be mentioned for better clarity. The steady state permeate flux increases with TMP at a particular Re and 'threshold TMP' is defined as the maximum TMP until the flux-TMP relation is linear (Bacchin et al. 2006; Field and Pearce 2011; Mondal and De 2018). Thus, the threshold TMP is always less than the limiting TMP. At a particular Re, permeate flux cannot be increases beyond limiting TMP. During microfiltration of tea extract, the variation of the steady state permeate flux with TMP at different Re is shown in Fig. 13.1(a) that shows excellent agreement of the calculated flux values with the experimental results. Also, the effect of TMP is more pronounced compared to Re. The limiting and threshold TMP calculated as discussed (Eq. 13.10) are plotted against Re in Fig. 13.1b. The limiting TMP increases slightly from 141 to 147 kPa with the increase in Re from 94 to 282 which indicates that the limiting TMP is delayed at higher Re. The threshold TMP also increases with Re at a faster rate and at higher Re approaches the limiting TMP.
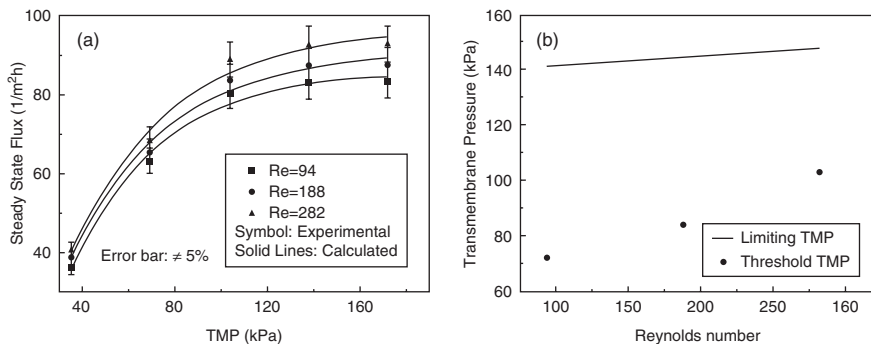
Fig. 13.1 Variation of (**a**) steady state flux with TMP at different *Re* and (**b**) limiting and threshold TMP with *Re*. (Reproduced from (Mondal and De 2018) with permission from Elsevier Science and Technology Copyright 2018)

Resistance in Series Model with Pore Blocking

Roy et al., have used the resistance in series model for quantifying the flux decline during ultrafiltration of Stevia extract using novel cellulose acetate pthalate-polyacrylonitrile blend membranes (Roy and De 2015). Their model considered additional resistance component (pore blocking, R_P) corresponding to the irreversible fouling, which was neglected in the model presented in the preceding section due to their small magnitude. The experimental permeate flux decline data provide a clue whether the pore blocking resistance, R_p needs to be considered or not. If there is a rapid decline of the permeate flux in initial few minutes of the experiments followed by a gradual decline that indicates that the membrane pore blocking by the solutes is prevalent during initial period of the filtration causing rapid flux decline in short term. Once pores are blocked, the solutes start depositing over the membrane surface growing with time slowly leading to the gradual flux decline in the long term. According to the study of Roy and De, such experimental flux decline trend was observed (Roy and De 2015). They observed that pore blocking was prevalent up to 125 s from the start of the experiments for various operating conditions. As discussed earlier, the pore blocking resistance during N^{th} experiment was estimated as follows:

$$R_P^N = \frac{\Delta P}{\mu J_w^N} - R_M^N \tag{13.11}$$

The above equation is valid for $0 < t < t_{PB}$, where t_{PB} is 125 s. Therefore, the overall flux decline during N^{th} is presented as:

$$J = \frac{\Delta P}{\mu \left(R_m^N + R_P^N(t) \right)} \quad \text{for} \quad 0 \leq t \leq t_{PB} \tag{13.12}$$

$$= \frac{\Delta P}{\mu\left(R_m^N + R_F^N\left(t - t_{PB}\right)\right)} \quad \text{for} \quad t_{PB} < t$$

The fouling resistance is expressed as (Roy and De 2015),

$$R_F^N(t) = R_F^{SN} - \left(R_F^{SN} - R_{PB}^N\left(t_{PB}\right)\right)\exp\left(-k_g\left(t - t_{PB}\right)\right) \tag{13.13}$$

It is interesting to note that the variation of membrane hydraulic resistance with number of experiments was correlated as:

$$R_m^N\left(m^{-1}\right) = 8.8 \times 10^{12}\, N^{0.42} \tag{13.14}$$

According to their study, the pore blocking resistance and the steady state fouling resistance had a trend with TMP and *Re* according to the following correlations (regressed over all the experiments),

$$\frac{R_{PB}^N}{R_m^N} = \left(2.4 \times 10^{-5} - 2.5 \times 10^{-7}\,\Delta P + 6.9 \times 10^{-10}\,\Delta P^2\right)\left(1.5 \times 10^5 - 0.6\,\mathrm{Re}\right) \tag{13.15}$$

$$\frac{R_F^{SN}}{R_m^N} = \left(40.4 - 0.26\,\Delta P + 4.9 \times 10^{-4}\,\Delta P^2\right)\exp\left(-1.2 \times 10^5\,\mathrm{Re}\right) \tag{13.16}$$

The steady state permeate flux for N^{th} experiment ($t \to \infty$) was expressed as follows:

$$J^{SN} = \frac{3.6 \times 10^9\,\Delta P}{\mu R_m^N\left[1 + \left(40.4 - 0.26\,\Delta P + 4.9 \times 10^{-4}\,\Delta P^2\right)\exp\left(-1.2 \times 10^5\,\mathrm{Re}\right)\right]} \tag{13.17}$$

where, the steady state flux is expressed as L/m²h and ΔP is in kPa, R_m^N is m⁻¹ and μ is in Pa.s. The limiting conditions were obtained as explained earlier ($\frac{dJ^{SN}}{d\Delta P} = 0$) and the relationship was given below.

$$\Delta P_{\lim}\left(kPa\right) = 45.3\sqrt{40 + \exp\left(1.23 \times 10^{-5}\,\mathrm{Re}\right)} \tag{13.18}$$

It was observed that the fouling resistance is a strong function of TMP but a weak function of *Re* (Roy and De 2015). The experimental data (scattered points) and modelled values (continuous line) are plotted in Fig. 13.2. The variation of steady-state permeate flux with TMP at different *Re* shows excellent corroboration between experimental and calculated values. The results presented in Fig. 13.3 support the previous observation that increase in *Re* delays the onset of limiting flux. The
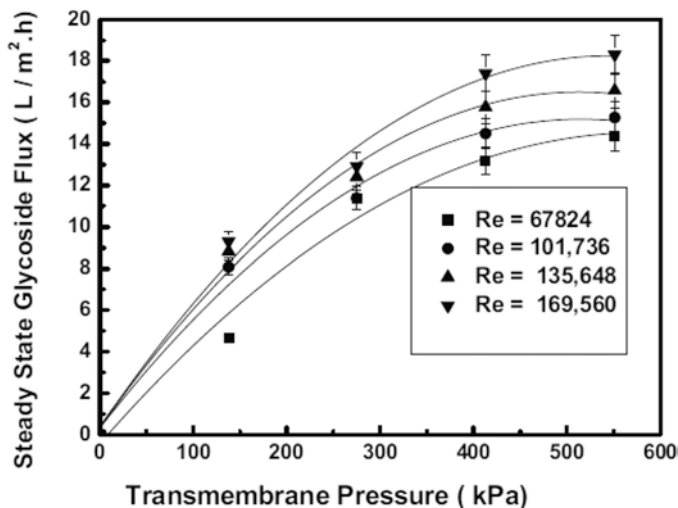
Fig. 13.2 Variation in steady state permeate flux with TMP and *Re*. (Reproduced from (Roy and De 2015) with permission from Elsevier Science and Technology Copyright 2015)
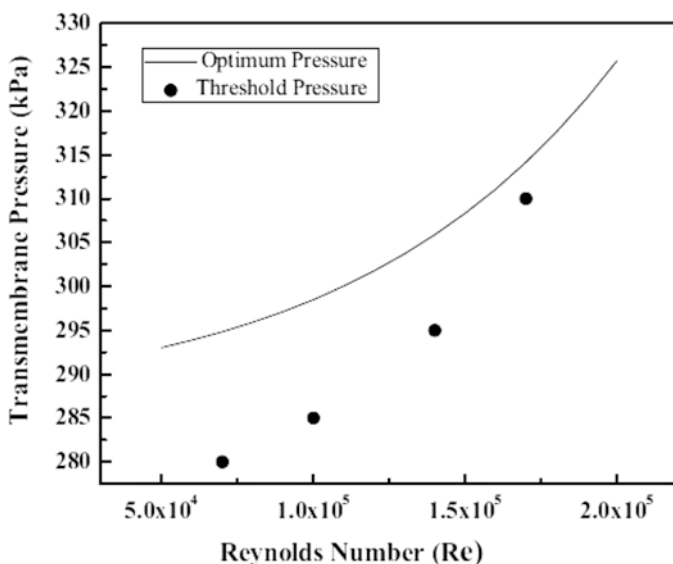

Fig. 13.3 Variation in limiting (Optimum) pressure and threshold. (Reproduced from (Roy and De 2015) with permission from Elsevier Science and Technology Copyright 2015)

threshold TMP is also showing similar trend with *Re*. The various parameters thus calculated can be an appropriate guide for selecting suitable operating conditions and design of scale up for specific applications.

2.2 Semi-empirical Models

Identification of the fouling mechanism is the first step in the process of developing any model from first principles. This can be done by carrying out filtration experiments at constant pressure either in a dead-end batch cell or a continuous cross flow cell. This section elaborates the different models available and their applications. The salient features of these models are they are semi-empirical in nature because they have a theoretical background for formulation. Some model parameters are estimated from the experimental data, imparting semi-empirical characteristics. However, the models are for quantification of the permeate flux decline behaviour, not for the estimation of the permeate concentration as a function of time.

2.2.1 Constant Pressure Dead End Filtration Cell (Batch Process): Hermia's Model

The prevalent flux decline mechanism can be identified by analyzing the characteristic curves of dead end batch cell using the equation (Hermia 1982; Ho and Zydney 2000)

$$\frac{dt^2}{dV^2} = k \left(\frac{dt}{dV} \right)^n \tag{13.19}$$

where, t and V are cumulative time and volume of the filtrate and k and n are model specific parameters. The parameter n assumes different values for various modes of filtration. It is 0 for the cake filtration, 1 for the intermediate pore blocking, 1.5 for the standard pore blocking and 2.0 for the complete pore blocking (Mondal et al. 2013). A schematic of different types of pore blocking mechanisms is presented in Fig. 13.4.

Complete Pore Blocking This is more common with solutes having molecular weight higher than the molecular weight cut-off (MWCO) of the membrane and the solute particles completely block the pores of the membrane (Fig. 13.4a). The permeate flux profile is given by (Bowen et al. 1995; Mondal et al. 2013)

$$J = J_0 \exp\left(-k_1 t \right) \tag{13.20}$$

where, J_0 and J are the initial and the permeate flux at any time t. k_1 is a constant related to the solute property.

Intermediate Pore Blocking In this mechanism, the particles do not have complete access to the pore and hence, deposit partly over already deposited solute particle (Fig. 13.4b). The permeate flux can be represented by (Bowen et al. 1995; Mondal et al. 2013)
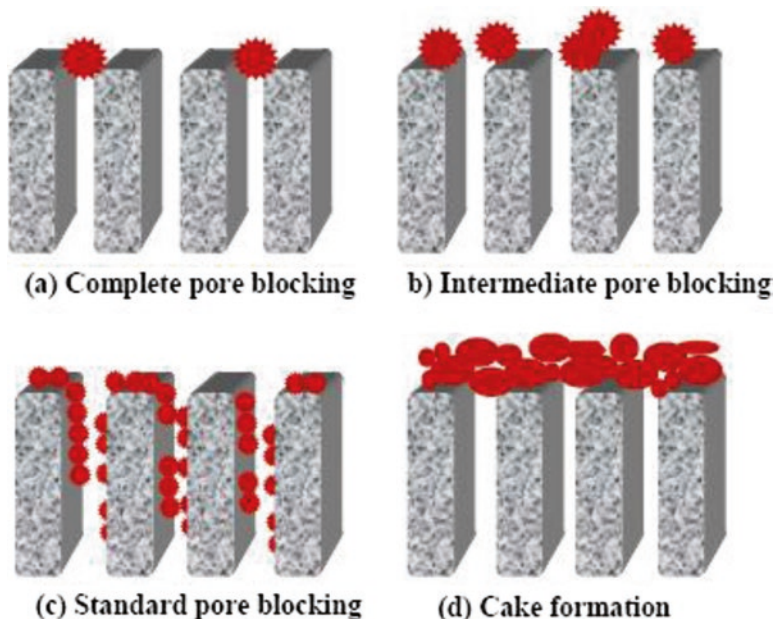
Fig. 13.4 Schematic of different pore blocking mechanisms. (**a**) Complete pore blocking. (**b**) Intermediate pore blocking. (**c**) Standard pore blocking. (**d**) Cake formation (Aghdam et al. 2015)

$$J = \frac{J_0}{\left(1 + k_2 t\right)} \tag{13.21}$$

k_2 is the model constant.

Standard Pore Blocking In this mechanism, solute particles deposit on the walls of the pores and therefore reduce the pore volume (Fig. 13.4c). The permeate flux decline can be represented as (Bowen et al. 1995; Mondal et al. 2013)

$$J = \frac{J_0}{\left(1 + \phi t\right)^2} \tag{13.22}$$

where, ϕ is the model constant.

Cake Filtration After initial filtration, the solute particles deposit over the blocked pores and form multiple layers of the solutes forming a cake layer over the membrane surface (Fig. 13.4d). Subsequently, this layer acts as the separation media and the porosity of this layer determines the permeate flux and quality. This mechanism is apparent at slightly later stage of filtration. The permeate flux during cake filtration is given as (Bowen et al. 1995; Mondal et al. 2013)

$$\frac{1}{J^2} = \frac{1}{J_0^2} + k_c t \qquad (13.23)$$

Hermia's model has been extensively used by several researchers during separation of bioactive compounds from fruit juices using batch mode membrane separation processes. Mondal et al., have used the model to study the fouling mechanism during filtration of Stevia extract suing ultrafiltration membranes (Mondal et al. 2013). They reported both intermediate pore blocking and cake filtration equally important for 100 kDa membrane. However, cake filtration mechanism was observed to be the dominant mechanism for lower MWCO ultrafiltration membranes, whereas pore blocking was more prevalent with the increase in MWCO of the membrane. They established that with the increase in membrane pore size, the probability of the pore blocking was increased. This is also supported by the findings of Reis et al., that indicates pore blocking as the dominant fouling mechanism for membranes with higher MWCO during the filtration of Stevia extract using ceramic microfiltration membranes (Reis et al. 2009). Mondal et al. have reported marginal variation in the ratio of cake resistance (R_c) to membrane hydraulic resistance (R_m) with transmembrane pressure (less than ±10%) indicating formation of an incompressible cake layer (Mondal et al. 2013). In case of compressible cake, R_c is a function of TMP, which is demonstrated in subsequent sections of this chapter. A response surface model was developed to estimate $\frac{R_c}{R_m}$ as a function of filtration time and MWCO of the membrane (Mondal et al. 2013). The model was observed to be in excellent agreement with the experimental data and shows an increase in $\frac{R_c}{R_m}$ with time due to the increase in cake layer thickness. This model can be used to predict the life of the membrane using pilot run data.

Aghdam et al. studied the filtration of pomegranate juice using membrane separation and identified cake filtration as the prevalent fouling mechanism (Aghdam et al. 2015). They reported the value of k_c with and without the application of ultrasound waves and established that even with the application of ultrasound waves, the fouling mechanism remained as cake formation. However, the intensity of cake formation was much lower in case of ultrasound waves. Gerke et al. attempted clarification of Yerba mate extract, a plant native to South America used as a digestive drink and reported that the cake filtration was the dominant mode of flux decline (Gerke et al. 2017). Other than internal pore blocking model, all other models were reported to be very close and as already discussed, in many cases they were very close to select the best fit. They also measured the relative magnitudes of different components of resistance using resistance in series model as explained in Sect. 2.1. The hydraulic resistance of the membrane remained unaltered with the operating conditions, whereas the resistance due to fouling varied with the operating pressure and flow rate. The variation of these parameters can be studied and used for design of scaled up version of the filtration system and also to determine the suitable operating conditions.

Rai et al. have studied the mechanism of permeate flux decline during microfiltration of watermelon juice in an unstirred batch cell using Hermia's model (Rai

et al. 2010). The experimental data was fit to the four models represented by Eqs. (13.20) to (13.23) in their linear form and the goodness of fit was compared using correlation coefficient as shown in Fig. 13.5. It was evident from the graph that cake filtration is the dominant mechanism caused by the build up of suspended solids and
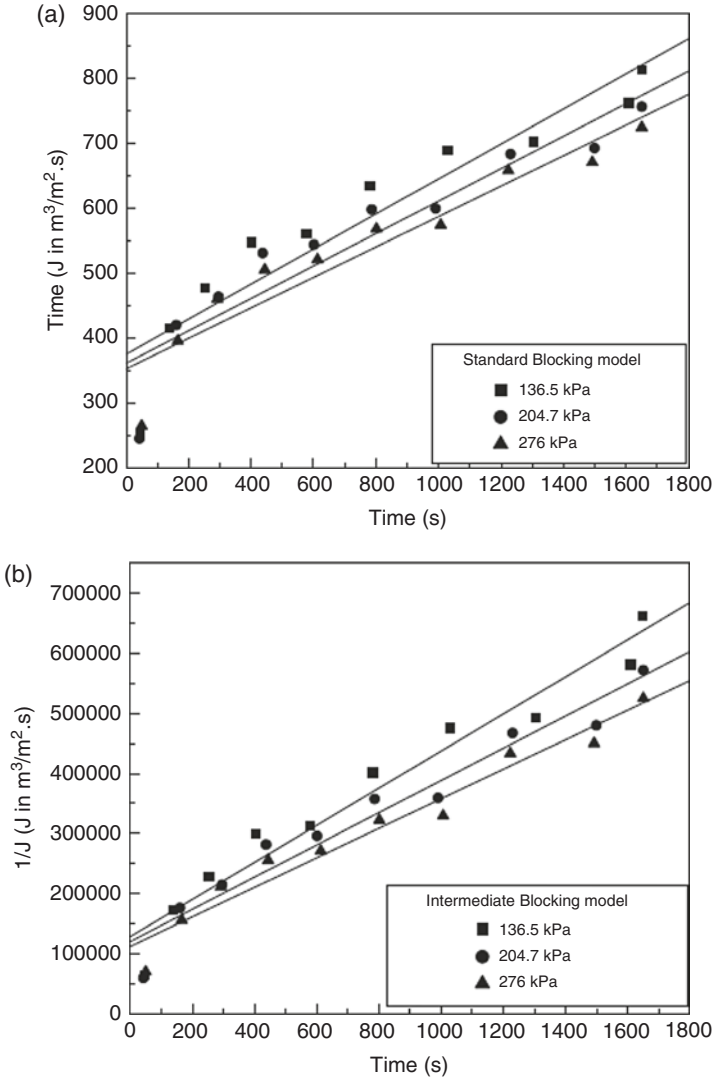
Fig. 13.5 Variation of (**a**) $n = 1.5$; $R^2 = 0.49$ to 0.52 $\dfrac{1}{\sqrt{J}}$ (**b**) $n = 1$; $R^2 = 0.57$ to 0.60 $\dfrac{1}{J}$ (**c**) $n = 2$; $R^2 = 0.37$ to 0.44 $\ln\left(\dfrac{1}{J}\right)$ and (**d**) $n = 0$; $R^2 = 0.96$ to 0.98 $\dfrac{1}{J^2}$ with time during microfiltration of watermelon juice in an unstirred batch cell. (Reproduced from (Rai et al. 2010) with permission from Springer Nature BV Copyright 2010)
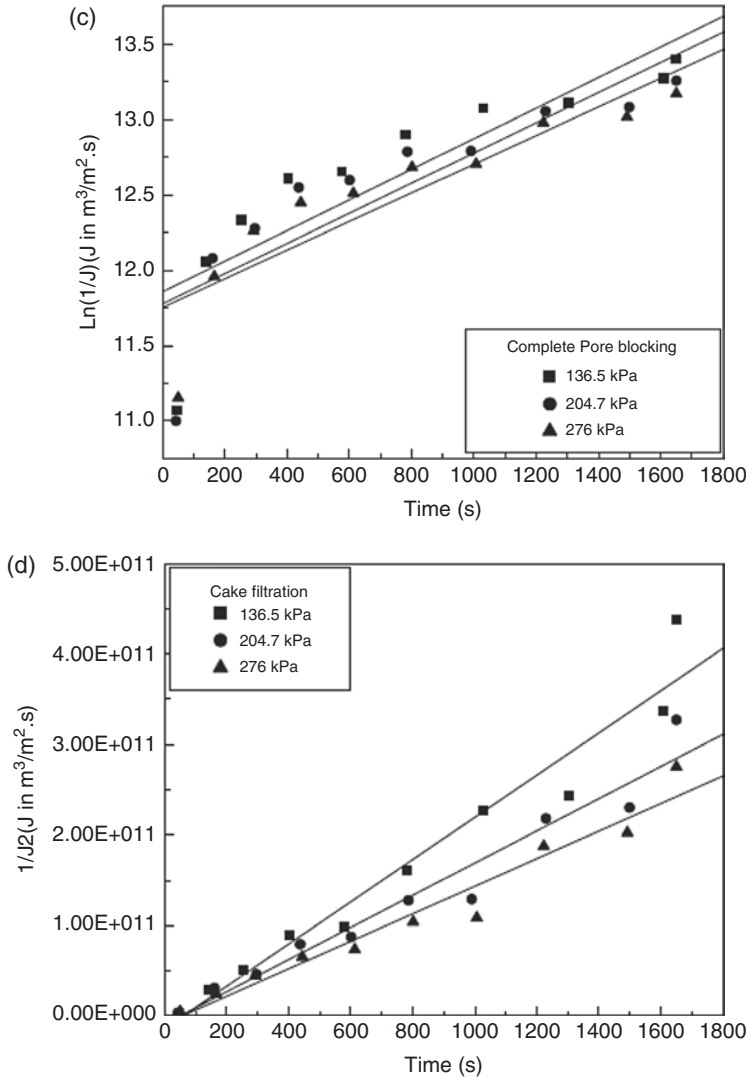
(c)

(d)

Fig. 13.5 (continued)

cell debris on the membrane surface. It may be mentioned that although the batch filtration is not industrially relevant, these models can be used to identify the mechanisms. However, they are useful for production of some high purity bioactive compounds that are expensive, and a low throughput is sufficient. Moreover, as mentioned previously, the modelling of batch filtration data for various models proposed by Hermia are sometimes too close to be differentiated statistically. In those cases, other physico-chemicals characterizations, like, scanning electron

microscopy of the cross section and top surface of the membrane before and after filtration with and without cleaning, as well as fourier transform infra red spectroscopy of the fresh and fouled membrane surface. These analyses would result into definite leads to understanding the prevailing mechanism of the membrane fouling (Jain et al. 2018).

2.2.2 Constant Pressure Cross Flow Filtration (Continuous Cross Flow Process): Field's Model

The flux decline models by Hermia for constant pressure dead end filtration is not applicable for cross flow filtration due to the presence of steady state flux (Mondal and De 2010). These models were modified by Field et al. for cross flow filtration (Field et al. 1995). Field's model was further used by several researchers for analyzing the filtration of bioactives using membrane separation (De Barros et al. 2003; Rai et al. 2006). According to this model, various mechanisms can be expressed by the generalized equation (Field et al. 1995)

$$\frac{dJ}{dt} = -k'\left(J - J^s\right)J^{2-m} \tag{13.24}$$

Similar to Eq. (13.19), the value and unit of k' and m depend on the mechanism of flux decline. For complete pore blocking ($m = 2$) and the flux decline is given by (Field et al. 1995; Rai et al. 2006):

$$J = J^s + \left(J_0 - J^s\right)e^{-k't} \tag{13.25}$$

For partial pore blocking ($m = 1$), the flux decline is expressed as:

$$k't = -\ln\frac{\left(J - J^s\right)J_0}{\left(J_0 - J^s\right)J} \tag{13.26}$$

For cake filtration ($m = 0$), the expression for flux decline is:

$$k't = \frac{1}{J^{s2}}\left[\ln\left(\frac{J}{J_0}\frac{\left(J_0 - J^s\right)}{\left(J - J^s\right)}\right) - J^s\left(\frac{1}{J} - \frac{1}{J_0}\right)\right] \tag{13.27}$$

Rai et al. used this model to analyse the cross flow ultrafiltration of depectinized mosambi juice (Rai et al. 2006). They observed that partial or complete pore blocking in the first few minutes of filtration followed the cake filtration model. However, they analysed considering only one mechanism for the entire duration and reported

the cake filtration as the dominant mechanism. Barros et al., studied the fouling behaviour of cross flow ultrafiltration of depectinized pineapple juice using the modified Field's model (De Barros et al. 2003). Similar analysis was carried out by Cassano et al. during the filtration of blood orange juice and reported standard pore blocking at lower *Re* and complete pore blocking at higher *Re* (Cassano et al. 2007).

All these studies reported the presence of two fouling mechanisms but analyzed using a single model throughout the entire duration of the filtration. In an actual filtration, it is likely that more than one mechanism act sequentially with a smooth transition at a particular time. In this regard, Mondal et al. have contributed significantly by proposing integrated models for characterization of the sequential fouling mechanisms (Mondal and De 2009, 2010). In the first work, they proposed the sequential occurrence of complete pore blocking followed by the cake filtration (Mondal and De 2009). With a rigorous mathematical treatment, they have developed a phase space defining three non-dimensional parameters that involved the combinations of the operating conditions as well as the model constants for the fouling mechanisms (Fig. 13.6a). The phase space clearly identified the three regions, the dominant complete pore blocking, comparable complete pore blocking and cake filtration and dominant cake filtration. Thus, one simply needs to evaluate these parameters from the operating conditions and the model parameters and confirm the prevalent membrane fouling mechanism. They gave a demonstration of the experimental data of pineapple juice filtration by Barros et al., and showed that the filtration was cake formation controlling at lower TMP and at higher TMP both cake filtration and complete pore blocking were important for the ceramic membrane used for the filtration (De Barros et al. 2003). Similar analysis was carried out for a sequential fouling by intermediate pore blocking and cake filtration (Mondal and De 2010). In this work, they also identified three non-dimensional parameters in terms of the operating conditions and the model parameters and generated a phase space plot (Fig. 13.6b) identifying the intermediate pore blocking controlling, both equally important and cake filtration controlling regions. They demonstrated this model for the filtration of the oily wastewater solution. They concluded that the increase in TMP led to dominant pore blocking, whereas increase in cross flow rate favoured cake controlling region, although the region of pore blocking controlling and both mechanisms controlling were really narrow. Therefore, by the generated phase space plot of sequential fouling mechanisms, one can identify the operating conditions so that the filtration can be belonging to the desirable controlling regime so that the permeate flux decline can be minimized.

A generalized formulation considering the simultaneous occurrence of complete pore blocking and intermediate pore blocking followed by cake filtration is useful in understanding the pore blocking mechanism. It is reasonable to consider that pore blocking proceeds from the beginning of the experiment up to a certain time of operation (t_{PB}) beyond which cake formation starts. Once the cake formation starts, solute particles start depositing over the membrane surface and there is hardly any scope of pore blocking to take place. As described earlier (Eq. 13.19), in the case of complete and intermediate pore blocking (till $t < t_{PB}$), the flux decline is described by Eqs. (13.20) and (13.21).
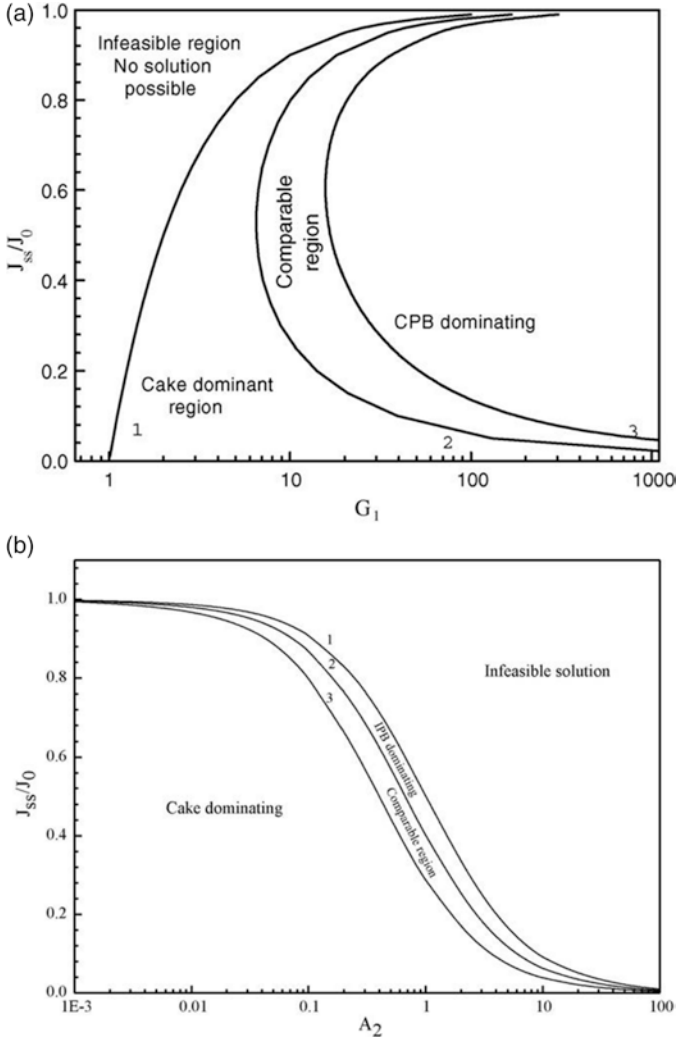
Fig. 13.6 Dominant filtration regimes in case of (**a**) complete pore blocking followed by cake formation (Reproduced from (Mondal and De 2009) with permission from Elsevier Science and Technology Copyright 2009) and (**b**) intermediate pore blocking followed by cake formation. (Reproduced from (Mondal and De 2010) with permission from Elsevier Science and Technology Copyright 2010)

In terms of resistance, the pore blocking resistances were defined as,

$$R_{CPB}^{*} = \frac{R_{CPB}}{R_m} = \exp(k_1 t) - 1 \tag{13.28}$$

$$R_{IPB}^* = \frac{R_{IPB}}{R_m} = J_0 k_2 t \tag{13.29}$$

The growth of cake resistance (for $t < t_{PB}$) is restricted due to external cross flow of the feed. In this case, the flux decline equation is obtained from Eq. (13.24) (Field et al. 1995). In terms of resistance, the expression of the flux becomes at $t > t_{PB}$,

$$J = \frac{\Delta P}{\mu \left[R_m + R_{CPB}\left(t_{PB}\right) + R_{IPB}\left(t_{PB}\right) + R_c\left(t - t_{PB}\right) \right]} \tag{13.30}$$

The above equation can be expressed in terms of non-dimensional resistances as:

$$J = \frac{J_0}{\left[1 + R_{CPB}^* + R_{IPB}^* + R_c^* \right]} \tag{13.31}$$

Permeate flux at time $t = t_{PB}$ is obtained as:

$$J_{t_{PB}} = \frac{J_0}{\left[1 + R_{CPB}^*\left(t_{PB}\right) + R_{IPB}^*\left(t_{PB}\right) \right]} \tag{13.32}$$

Combining the above two equations, the following expression is obtained,

$$J = \frac{J_{t_{PB}}}{1 + R_c^{**}} \tag{13.33}$$

where, R_c^{**} is defined as:

$$R_c^{**} = \frac{R_c^*}{\left[1 + R_{CPB}^*\left(t_{PB}\right) + R_{IPB}^*\left(t_{PB}\right) \right]} \tag{13.34}$$

Taking the derivative of equation Eq. (13.34) with respect to t, the rate of flux change is obtained as:

$$\frac{dJ}{dt} = -\frac{J_{t_{PB}}}{\left(1 + R_c^{**}\right)^2} \frac{dR_c^{**}}{dt} \tag{13.35}$$

Using Eqs. (13.31) and (13.34), the governing equation of cake resistance is obtained,

$$\frac{dR_c^{**}}{dt} = \frac{J_{t_{PB}} k_c}{\left(1 + R_c^{**}\right)} \left[J_{t_{PB}} - J_{ss} \left(1 + R_c^{**}\right) \right] \tag{13.36}$$

At steady state, $\dfrac{dR_c^{**}}{dt} = 0$ and therefore, from Eq. (13.36), the following criterion at the steady state is obtained,

$$J_{t_{PB}} = J_{ss} \left(1 + R_{cs}^{**}\right) \tag{13.37}$$

Considering Eqs. (13.31), (13.32), (13.33), (13.34), Eq. (13.37) can be transformed as follows:

$$R_c^* = \frac{J_0}{J_{ss}} - \left(1 + R_{CPB}^* + R_{IPB}^*\right) \tag{13.38}$$

From the continuity equations at $t = t_{PB}$, the flux obtained through both the mechanisms would be equal, which implies,

$$\left.\frac{dJ}{dt}\right|_{t=t_{PB}-\Delta t} = \left.\frac{dJ}{dt}\right|_{t=t_{PB}+\Delta t} \tag{13.39}$$

Using Eqs. (13.20), (13.21) and (13.23) in Eq. (13.39), we obtain,

$$k_1 \exp\left(k_1 t_{PB}\right) + J_0 k_2 = J_0 k_c \left(J_{t_{PB}} - J_{ss}\right) \tag{13.40}$$

Selecting non-dimensional parameters as $k_1 t_{PB} = \tau, \dfrac{k_c J_0^2}{k_1} = G_1$ and $\dfrac{J_0 k_2}{k_1} = G_2$, Eq. (13.40) can be written as:

$$\exp(\tau) + G_2 = G_1 \left(\frac{1}{\exp(\tau) + G_2 \tau} - \frac{J_{ss}}{J_0} \right) \tag{13.41}$$

Comparison of Resistances Since, from Eqs. (13.28) and (13.29), complete and intermediate pore blocking resistances are quantified. Therefore,

$$\frac{R_c^*}{R_{IPB}^*} = \frac{1}{J_0 k_2 t_{PB}} \left[\frac{J_0}{J_{ss}} - \exp\left(k_1 t_{PB}\right) \right] - 1 \tag{13.42}$$

In terms of non-dimensional terms (using Eq. 13.41) Eq. (13.42) can be transformed to

$$\frac{R_c}{R_{IPB}} = \frac{\left(e^\tau + G_2\right)\left(e^\tau + G_2\tau\right)^2}{G_2\tau\left[G_1 - \left(e^\tau + G_2\right)\left(e^\tau + G_2\tau\right)\right]} \tag{13.43}$$

Similarly, $\dfrac{R_c}{R_{IPB}}$, $\dfrac{R_c}{R_{CPB} + R_{IPB}}$ and $\dfrac{R_{CPB}}{R_{IPB}}$ can be obtained as:

$$\frac{R_c}{R_{CPB}} = \frac{1}{\left(e^\tau - 1\right)}\left[\frac{G_1 G_2 \tau + \left(e^\tau + G_2\right)\left(e^\tau + G_2\tau\right)}{G_1 - \left(e^\tau + G_2\right)\left(e^\tau + G_2\tau\right)}\right] \tag{13.44}$$

$$\frac{R_c}{R_{CPB} + R_{IPB}} = \frac{1}{\left(e^\tau + G_2\tau - 1\right)}\left[\frac{\left(e^\tau + G_2\right)\left(e^\tau + G_2\tau\right)^2}{G_1 - \left(e^\tau + G_2\right)\left(e^\tau + G_2\tau\right)}\right] \tag{13.45}$$

$$\frac{R_{CPB}}{R_{IPB}} = \frac{e^\tau - 1}{G_2\tau} \tag{13.46}$$

Relative dominance of the each of these resistances can be compared by setting the values of the ratios to be greater or less than unity.

Infeasible solution will result when $\dfrac{R_c}{R_{CPB}}$, $\dfrac{R_c}{R_{IPB}}$, $\dfrac{R_c}{R_{CPB} + R_{IPB}}$ and $\dfrac{R_{CPB}}{R_{IPB}} < 0$. Considering Eqs. (13.43), (13.44), (13.45), and (13.46), the necessary and sufficient condition for infeasibility is:

$$\frac{G_1}{e^\tau + G_2} < e^\tau + G_2\tau < 1 \tag{13.47}$$

for all positive real solutions of τ from Eq. (13.41).

Figure 13.7 shows the infeasibility boundary of τ in the parameter space by solving Eq. (13.41). The region above the curves shows the realistic solution of τ for different combinations of G_1 and G_2. So, for existence of the fouling mechanisms one has to select G_1, G_2 and J_{ss}/J_0 suitably. Solution of τ in the feasible domain is presented in Fig. 13.8. Using the values of τ and the parameters (G_1, G_2 and J_{ss}/J_0) relative dominance of the blocking mechanism during filtration can be identified, for the instances of only complete pore blocking followed by cake formation and only intermediate pore blocking followed by cake filtration (Mondal and De 2009, 2010). The regimes of dominant fouling mechanisms are already shown in Fig. 13.6. An operator can preset these values of the parameters within the feasible boundary of τ to operate the cross-flow filtration in a preferential fouling regime.
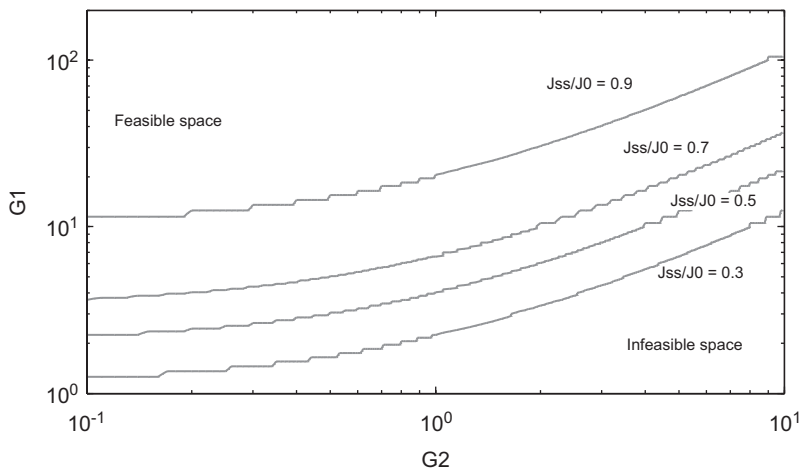
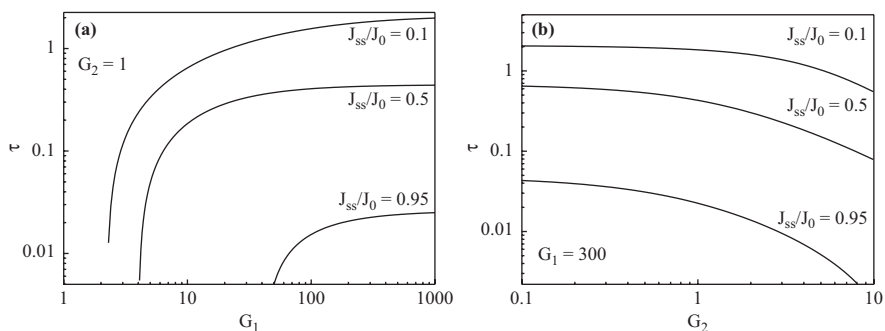**Fig. 13.7** Infeasibility regimes of solution of τ in the parameter space

Fig. 13.8 Real solution of τ by solving Eq. (13.41) in the feasible domain of G_1, G_2 and J_{ss}/J_0 varying (**a**) G_1, keeping G_2 fixed and (**b**) G_2, keeping G_1 fixed

2.3   Transport Phenomena-Based Models

This section presents detailed discussion on modelling of ultrafiltration process derived from the first principles. They are broadly divided into two subsections, namely, (1) modelling of permeate flux and concentration and (2) modelling of permeability hysteresis.

2.3.1   Modelling of Permeate Flux and Concentration

The class of the models discussed earlier are incapable to predict the permeate flux and permeate concentration simultaneously. This can be achieved by the transport phenomena-based models. The main aim of ultrafiltration of fruit juices and

bioactive compounds is to remove different proteins, pectin, microbes and maximum permeation of nutrients and minerals. As discussed, the major challenge during this is the membrane fouling resulting in inconsistency in throughput as well as product quality. Mondal et al., have attempted to model the performance of the ultrafiltration of Stevia extract in cross flow (Mondal et al. 2013). The complexity arising in case of real-life effluents is the fact that in these cases, the feed stream comprises of a mixture of components and the transport properties viz., diffusivities and gel properties are not known. Mondal et al. have used the experimental results to estimate these parameters through optimization techniques and flux decline as well as concentration profile of the permeate stream are predicted using the model (Mondal et al. 2012a, 2013). This section is divided into three subsections viz., (1) modelling for the total recycle mode and (2) batch concentration mode.

Total Recycle Mode
Steady State Model

Mondal et al. assumed that the Stevia extract was a mixture of high molecular weight (HMW) components (proteins, polysaccharides etc.,) and low molecular weight (LMW) solutes (Steviosides etc.,) (Mondal et al. 2013). The HMW solutes were retained by the membrane forming a gel layer on the membrane surface. LMW solute like Stevioside (804.87 g/mol) was partially retained by the gel layer. The system under consideration along with the co-ordinate system is shown in Fig. 13.9, where, $y = 0$ and $y = \delta$ signify the two interfaces of the concentration boundary layer and L is the gel layer thickness. $y = 0$ indicates the bulk of the solution and $y = \delta$ shows the concentration boundary layer and gel layer interface.

All the experiments were conductedin rectangular cross flow set up and both permeate and retentate were recycled back to the feed tank. The HMW solute was the main constituent of the gel layer and hence, the steady state permeate flux (J) was expressed from the classical film theory as:

$$J = k_f \ln\left(\frac{C_{1g}}{C_{1b}}\right) \tag{13.48}$$

In the above expression, C_{1g} and C_{1b} are concentration of component 1 (HMW solutes) in gel layer and bulk, respectively. k_f is the mass transfer coefficient and can be estimated from the standard Sherwood number correlations, as follows:

$$Sh = \frac{k_f d_e}{D_1} = 1.85\left(Re\,Sc\frac{d_e}{l}\right)^{\frac{1}{3}} \quad for \ \ Re < 2100 \tag{13.49}$$

where, l is the characteristic length of the system, Sh, Re, and Sc are Sherwood, Reynolds, and Schmidt number corresponding to component 1. In an ideal gel controlling filtration model, the mass transfer coefficient is independent of TMP (Trettin and Doshi 1980). But several literatures reported that the mass transfer coefficient shows a weak dependence on TMP for membrane systems (Gekas and Hallström
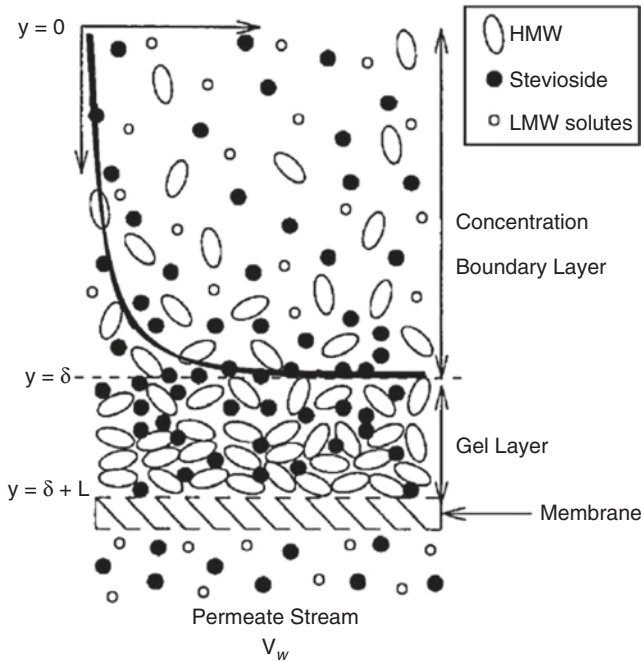
Fig. 13.9 Schematic of transport of mixed solutes through ultrafiltration membrane. (Reproduced from (Mondal et al. 2012b) with permission from Elsevier Science and Technology Copyright 2012)

1987; Johnston and Deen 2002; Mondal et al. 2011). Thus, the following expression of permeate flux was proposed.

$$J = k_{f1} \ln \left(\frac{C_{1g}}{C_{1b}} \right) \tag{13.50}$$

where, $k_{f1} = k_f(a + b\Delta P)$. The four parameters, namely, a, b, C_{1g} and D_1 (diffusivity of component 1) were estimated through optimization routine by minimizing the sum of square of errors (S_0) of permeate flux defined as:

$$S_0 = \sum_{i=1}^{N_{exp}} \left[\frac{J_{exp}^i - J_{cal}^i}{J_{exp}^i} \right]^2 \tag{13.51}$$

In the above equation, J_i^{exp} and J_i^{cal} were the experimental and calculated flux of the ith experiment. The estimated parameters were $D_1 = 3.7 \times 10^{-11}$ m²/s, $C_g = 51.5$ kg/m³, $a = 0.35$ and $b = 1.22 \times 10^{-6}$ Pa⁻¹. A comparative analysis of the model predicted permeate flux with experimental results is presented in Fig. 13.10 that shows reasonable agreement between the two ($\pm < 15\%$).
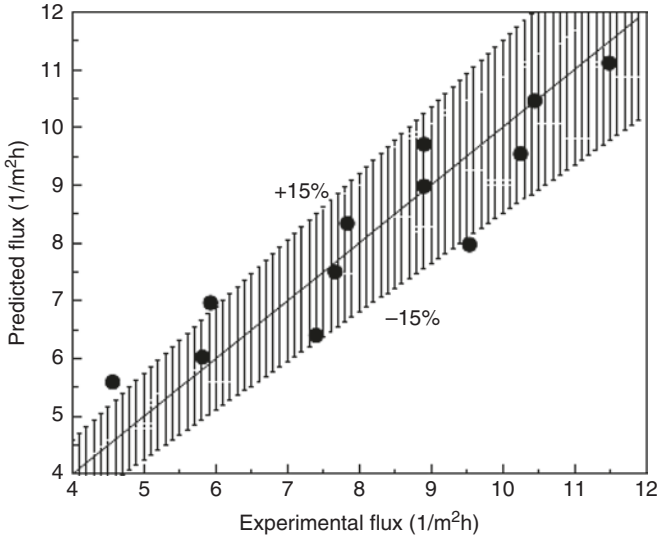
Fig. 13.10 Comparison of model predicted flux with experimental results for steady state ultrafiltration in total recycle mode. (Reproduced from (Mondal et al. 2012b) with permission from Elsevier Science and Technology Copyright 2012)

Transient Model

The mass balance of HMW solutes in the mass transfer boundary layer $(0 < y < \delta)$ as shown in Fig. 13.6 results in the following equation de (De and Bhattacharya 1997)

$$\rho_g \left(1 - \varepsilon_g\right) \frac{dL}{dt} = J_w C_1 - D_1 \frac{dC_1}{dy} \tag{13.52}$$

where, ε_g and ρ_g are porosity and density of the gel layer. Integrating the above equation, within the limits, $y = 0$, $C_1 = C_{1b}$ and $y = \delta$, $C_1 = C_{1g}$ results in

$$\rho_g \left(1 - \varepsilon_g\right) \frac{dL}{dt} = J_w \frac{C_{1g} - C_{1b} \exp\left(\dfrac{J_w}{k_{f1}}\right)}{1 - \exp\left(\dfrac{J_w}{k_{f1}}\right)} \tag{13.53}$$

Similarly, mass balance of LMW solute (i.e., Stevioside) was carried out in the mass transfer boundary layer as well as gel layer, and following the derivation of De and Bhattacharyya, the concentration of Stevioside on the membrane surface can be expressed as (De and Bhattacharya 1997):

$$C_{2m} = \frac{C_{2b} \exp\left[J_w \left(\left(\dfrac{1}{k_{f2}}\right) + \left(\dfrac{L}{\varepsilon_g D_2}\right)\right)\right]}{\gamma_g R_{r2} + \left(1 - R_{r2}\right)\left(\gamma_g - 1\right) \exp\left(\dfrac{J_w L}{\varepsilon_g D_2}\right) + \left(1 - R_{r2}\right) \exp\left[J_w \left(\left(\dfrac{1}{k_{f2}}\right) + \left(\dfrac{L}{\varepsilon_g D_2}\right)\right)\right]} \tag{13.54}$$

In the above expression, $R_{r2}\left(=1-\dfrac{C_{2p}}{C_{2m}}\right)$ is the real retention of Stevioside and

γ_g is the partition coefficient defined as $C_2(\delta^-) = \gamma_g C_2(\delta^+)$. The variation in concentration of Stevioside across the membrane results into osmotic pressure difference given as $\Delta\pi = \pi_m - \pi_p$. The osmotic pressure (π) can be expressed in terms of concentration from van't Hoff's relation $\pi = \dfrac{RT}{M_w}C$ that can be written as:

$$\Delta\pi = \frac{RT}{M_{2b}}C_{2m}R_{r2} \tag{13.55}$$

In the above equation, R is the universal gas constant, M_w is the molecular weight of the solute and T is the temperature in Kelvin scale. Hence, the permeate flux at any time instant can be written as

$$J_w(t) = \frac{\Delta P - \Delta\pi}{\mu\left(R_m + R_g\right)} \tag{13.56}$$

where, R_m and R_g are resistance offered by the membrane and the gel layer, respectively. According to the classical cake filtration model,

$$R_g = \beta L \tag{13.57}$$

and $\beta = \alpha(1 - \varepsilon_g)\rho_g$ is a constant and the characteristic of the gel layer. α is the specific gel resistance. There are five parameters $(D_2, \rho_g, \beta, \gamma_g$ and $\varepsilon_g)$ to be estimated using the five algebraic equations represented by Eqs. (13.53), (13.54), (13.55), (13.56), and (13.57). R_{r2} was determined using dead end batch cell under high stirring and it was found to be 0.1. The remaining parameters were estimated by minimizing the sum of square of errors between the experimental and calculated values for permeate flux and Stevioside concentration represented as:

$$S_1 = \sum_j^{N_2}\sum_i^{N_j}\left[\frac{J_{w,cal}^{ij} - J_{w,exp}^{ij}}{J_{w,exp}^{ij}}\right]^2 + \sum_{k=1}^{N_p}\left[\frac{\overline{C}_{2p,cal}^k - \overline{C}_{2p,exp}^k}{\overline{C}_{2p,exp}^k}\right]^2 \tag{13.58}$$

In above equation, i and j represent the number of experimental data points and number of experiments, respectively. N_j represents the number of data at various time instants in jth experiment and N_p is the number of experiments at a particular TMP. Stevioside concentration of the cumulative permeate was measured at the end of each experiment and hence, the average Stevioside concentration in the permeate can be calculated from

$$\overline{C}_{2p} = \overline{C}_{2m}\left(1 - R_{r2}\right) \tag{13.59}$$

$$\overline{C}_{2p} = \frac{1}{t}\left(1 - R_{r2}\right)\int_0^t C_{2m}dt \tag{13.60}$$

where, $\overline{C_{2p}}$ and $\overline{C_{2m}}$ are time averaged concentration of Stevioside in permeate and on the membrane surface, respectively. The estimated five parameters were: $D_1 = 2 \times 10^{-11}$ m^2/s, $\varepsilon_g = 0.56$, $\rho_g = 1550$ kg/m^3, $\gamma_g = 3.15$ (averaged) and $\beta = 4.55 \times 10^{19}$ m^{-2} (Mondal et al. 2012b). The study of Mondal et al., for filtration of Stevia extract showed that the parameters, β and ε_g were invariant with pressure whereas, γ_g was observed to be varying with pressure in the range of 2.25 to 6.13 (Mondal et al. 2012b). According to their study, at higher TMP, gel layer retains more Stevioside. With the optimized parameters, the profiles of the permeate flux, Stevioside concentration, gel layer thickness and gel layer resistance were calculated. Effect of TMP and CFR on the gel layer thickness is presented in Fig. 13.11. As evident from the figure, with the progress of filtration, the gel layer thickness increases and permeate flux decreases. Finally, the gel layer growth is arrested due to the forced convection imposed by the crossflow velocity. Similarly, increase in CFR results into decrease in the growth of gel layer. Increase in gel layer thickness with TMP can be explained by the enhanced convection of gel forming solutes towards membrane surface at higher pressure.

Figure 13.12 shows the calculated and the experimental permeate flux profiles for a typical set of operating conditions. It is observed that the model adequately describes the permeate flux decline.

The predicted and experimental Stevioside concentration in the permeate for different operating conditions are presented in Table 13.1.

Mondal and De have prepared novel ultrafiltration hollow fiber membranes by blending polyvinylidene fluoride with polysulfone (PSf) for purification of polyphenols and EGCG from green tea extract (Mondal and De 2019). In their work, they also utilized the same model with satisfactory prediction of the permeate flux decline, as well as the polyphenol concentration in the permeate.

Fig. 13.11 Model predicted profile of gel layer thickness. (Reproduced from (Mondal et al. 2012b) with permission from Elsevier Science and Technology Copyright 2012)
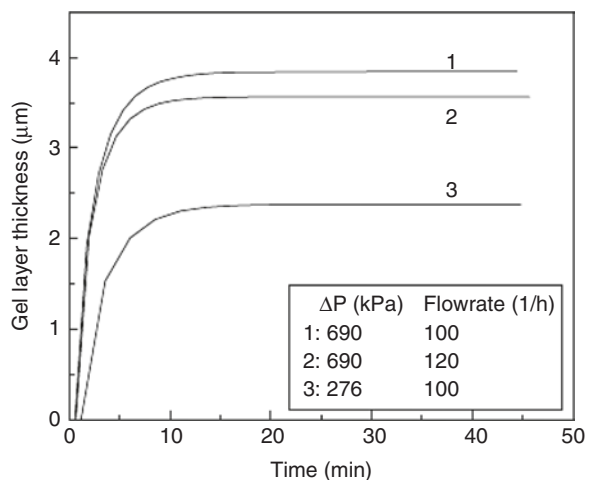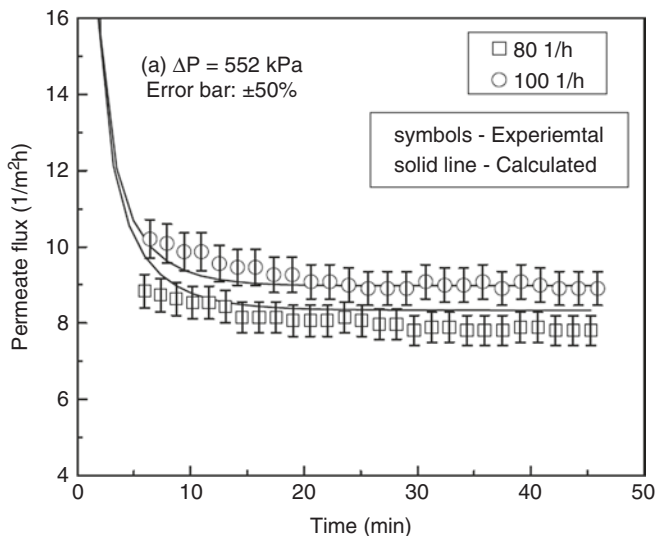
Fig. 13.12 Transient permeate flux profiles (both experimental and calculated). (Reproduced from (Mondal et al. 2012b) with permission from Elsevier Science and Technology Copyright 2012)

Table 13.1 Comparison of the experimental and predicted Stevioside concentration in the permeate for various operating conditions (Mondal et al. 2012b)

TMP (kPa)	80 LPH		100 LPH		120 LPH	
	Predicted	Experiment	Predicted	Experiment	Predicted	Experiment
276	51.6	58.0	51.4	49.0	51.3	49.0
414	43.0	45.0	42.7	43.3	42.5	40.4
552	39.3	40.5	39.0	39.7	38.9	37.3
690	29.5	29.7	29.3	31.1	29.1	27.5

Batch Concentration Mode

In this mode of operation, permeate is not recycled back but is withdrawn continuously leading to the continuous increase in concentration of the feed stream. This in turn leads to increase in gel layer thickness, which is a direct function of feed concentration. Therefore, in this mode, there is a significant flux decline as compared to total recycle mode. The total resistance to the filtration can be expressed as a sum of membrane hydraulic resistance (R_m), the resistance due to boundary layer (R_{bl}) and the gel layer resistance (R_g) (Mondal et al. 2012b).

$$R_T = R_m + R_g + R_{bl} \tag{13.61}$$

The average value of permeate flux is higher in total recycle mode than the batch mode under identical operating conditions and mass transfer coefficient is inversely

proportional to the boundary layer resistance. Therefore, mathematically, it may be expressed as $R_T^r < R_T^b$ and $k_{f1}^b < k_{f1}^r$, where, the subscripts b and r represent batch and total recycle mode, respectively. Simultaneously, due to deposition of gel layer over membrane surface the effective channel height ($2h$) decreases resulting into increased cross flow velocity (u). Mass transfer coefficient in batch mode can be rearranged as

$$k_f^b = \left(\frac{uD_1^2}{d_e L} \right) \tag{13.62}$$

Increase of u in the batch mode results into the inequality, $k_f^b > k_f^r$. The effect of TMP on the mass transfer coefficient can be written as

$$k_{f1}^b = k_f^b \left(a_b + b_b \Delta P \right) \tag{13.63}$$

Considering the overall material balance, the following equation is obtained

$$\frac{d}{dt} \left(\rho_f V \right) = -J_w A_m \rho_p \tag{13.64}$$

where, V is the volume of the feed, ρ_f and ρ_p are feed an permeate densities and A_m is the effective area of the membrane. Considering the species balance of gel forming material we get,

$$\frac{d}{dt} \left(C_{1b} V \right) = -J_w A_m C_{p1} \tag{13.65}$$

Considering that the permeate is devoid of any gel forming material, $C_{p1} = 0$ and using the boundary condition, at $t = 0$, $C = C_{01}$ and $V = V_0$ we get

$$C_{1b} = \frac{C_{01} V_0}{V} \tag{13.66}$$

The species balance of Stevioside results into

$$\tag{13.67}$$

$$C_{2b} \frac{dV}{dt} + V \frac{dC_{2b}}{dt} = -J_w A_m C_{p2}$$

with the initial condition, at $t = t_0$, $C = C_{02}$ and $V = V_0$. The deposition of gel layer increases with time accompanied by the decrease in effective channel height, that can be quantified using the gel layer thickness, L, as

$$d_e^t = d_e - 2L(t) \tag{13.68}$$

Corresponding cross flow velocity can be mathematically represented as:

$$u^t = \frac{Q}{w \times \left(d_e^t / 2 \right)} \tag{13.69}$$

where, w is the width of the filtration cell. The cross-flow velocity thus evaluated has been utilized to estimate the mass transfer coefficient (k_f^b). Using Eqs. (13.53), (13.54), (13.55), (13.56), and (13.57) and combining Eqs. (13.63), (13.64), (13.66) to (13.69), a system of differential-algebraic equations was set up. Solving the optimization function in Eq. (13.58), five state variables (L, C_{1b}, C_{2b}, C_{2m} and V) were calculated as function of time. The parameters, a_b and b_b were found to be 0.22 and 2.22×10^{-7} Pa^{-1} (Mondal et al. 2012b).

In this mode of operation, the volume of the feed decreased continuously due to extraction of permeate resulting to the increase in the volume concentration factor (VCF$=V_0/V(t)$). Figure 13.13 shows the variation of VCF with different operating conditions indicating a good match between the experimental data and the calculated ones.

The profiles of flux and the Stevioside concentration in the permeate are shown in Fig. 13.14.

The permeate flux exhibits steep decline in the first 100 min. of the filtration time and the profile predicted by the model is in excellent agreement with the experimental data. In this mode, since the volume of the feed decreases and at higher TMP more filtrate is taken out. This is being accounted by considering a volume correction factor, which attains value of 1.4 after 10 h of operation. Recovery of Stevioside in the permeate was estimated at various operating parameters and found to be in close agreement with the experimental results. In batch mode, as more solvent is withdrawn, the gel layer thickness increases retaining more Steviosides, thereby decreasing its concentration with the filtration time. Thus, it may be concluded that the proposed model, can be efficiently used to scale up filtration of Stevia extract and recovery of Stevioside both in total recycle and batch concentration mode.
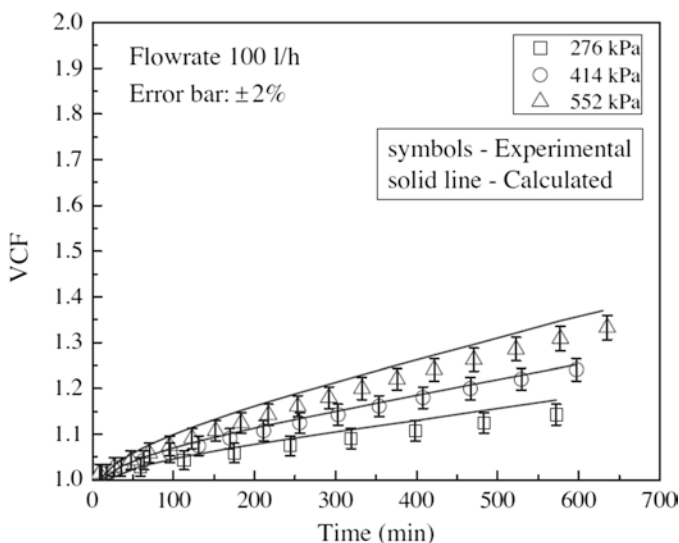
Fig. 13.13 Profiles of the VCF at different operating conditions. (Reproduced from (Mondal et al. 2012b) with permission from Elsevier Science and Technology Copyright 2012)
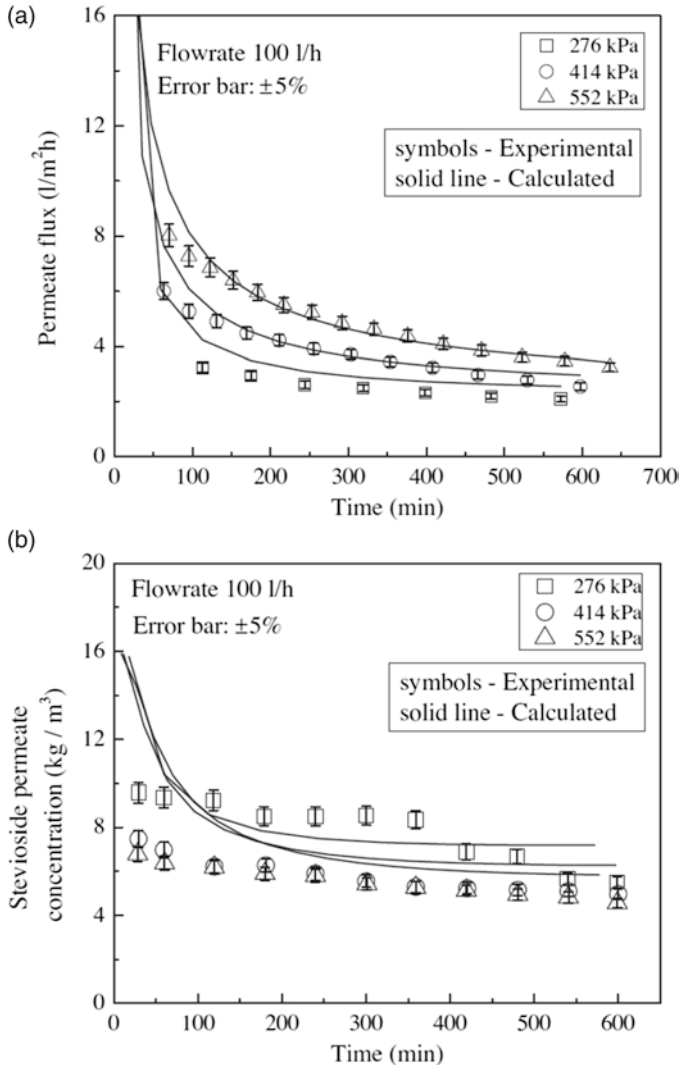
Fig. 13.14 Variation of profiles of flux and Stevioside in the permeate for different operating conditions. (Reproduced from (Mondal et al. 2012b) with permission from Elsevier Science and Technology Copyright 2012)

2.3.2 Permeate Flux Hysteresis

Real life solutions exist as a mixture of soluble and suspended substances consisting of LMW solutes such as vitamins, sugars, organic acids, as well as HMW solutes (such as proteins, pectins, cellulosic materials etc.) (Mondal et al. 2020). During filtration, some of the components may be rejected while some may permeate depending on the MWCO of the membrane. Typically, the HMW is retained on the membrane surface forming the gel layer. The permeate quality is dependent on the

size of the LMW components relative to the porosity of the gel layer and that of the membrane. The gel layer formed is compressible in nature and the thickness of the layer varies with the operating pressure. The linear flux-pressure relation deviates at higher pressure due to the consolidation of the gel layer. With increasing pressure cycle, the gel layer continuously grows, and the gel layer thickness is greater than the reducing pressure cycle. The pressure responsive variations in gel layer thickness result into hysteresis in the permeate flux during continuous operation of cross flow membrane system. Permeate flux hysteresis is a very significant aspect observed during the filtration of fruit juices for extraction of bioactive compounds. The quantification of permeate flux quantity and quality during the hysteresis is a key factor to be considered during scale up of the commercial units. However, the research in this area is scant and remains unexplored. In case of gel layer filtration operated below critical flux limit, Field et al. have reported the hysteresis in permeate flux (Field et al. 1995).

Mondal et al. have reported a detailed study on modelling of the transport of the HMW as well LMW solutes through the membrane for recovering phenolic compounds from clarified aqueous extracts of olive mill solid wastes (Mondal et al. 2020). The fundamental model used in their work was developed by De and Bhattacharya for ultrafiltration of a two component aqueous solution containing gel forming HMW and LMW solutes with known transport coefficients (De and Bhattacharya 1997). For actual fruit juices or plant extracts, independent determination of the system and model parameters is extremely difficult. Modelling approach adopted by Mondal et al. can predict the transport coefficient of permeating solutes in presence of gel forming solute for a continuous filtration of bioactives. The model also estimates the thickness of the gel layer, which is otherwise not possible to measure experimentally or analytically.

Membranes with High MWCO

In this model, component 1 is HMW and participates in the formation of gel layer. Component 2 is LMW and can permeate freely through the membrane, but their movement is hindered by the gel layer. The concentration profile of component 2 during filtration is shown in Fig. 13.15. Component 1 is retained on the membrane surface and forms the gel layer. At the steady state, the permeate flux (J_w) can be estimated from the film theory as (Blatt et al. 1970)

$$J_w = k_f \ln\left(\frac{C_{g1} - C_{p1}}{C_{01} - C_{p1}}\right) \tag{13.70}$$

where, k_f is the mass transfer coefficient and C_{g1}, C_{p1} and C_{01} are the concentration of component 1 in gel, permeate and bulk, respectively. k_f can be estimated from the theoretical Sherwood number (Sh) correlation, ignoring the effect of viscosity in the form,

$$Sh = \frac{k_f h}{D_1} = \xi \left(\text{Re}\, Sc\, \frac{h}{l}\right)^{\frac{1}{3}} \left(\frac{C_{g1}}{C_{01}}\right)^{\frac{1}{3}} \tag{13.71}$$
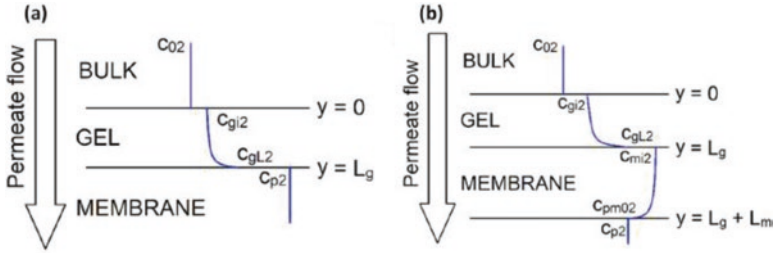
Fig. 13.15 Schematic of different membrane layers and concentration profile of 2nd component for membranes with (**a**) HMW and (**b**) LMW. (Reproduced from (Mondal et al. 2020) with permission from Elsevier Science and Technology Copyright 2020)

Table 13.2 Value of ξ for different geometries of the filtration module (Mondal et al. 2020)

Geometry	Classical Leveque solution (constant mass transfer boundary layer)	Considering developing mass transfer boundary layer
Rectangular	1.86	2.10
Tubular	1.62	1.816
Radial cross flow	1.47	1.65

where, *Re* and *Sc* are Reynolds and Schmidt number and *h* is the channel half-height. The value of the constant, ξ, depends on the geometry of the system and is presented in Table 13.2.

C_{p1} through the membrane can be obtained using the modified Kedem-Katchalsky equation (Katzir-Katchalsky and Curran 1965)

$$J_w C_{p1} = B_1 \left(C_{g1} - C_{p1} \right) + \left(1 - \sigma_1 \right) \bar{C}_1 v_w \tag{13.72}$$

where, $\bar{C}_1$ is the log mean average concentration of component 1 in the membrane represented as $\bar{C}_1 = \dfrac{C_{g1} - C_{p1}}{\ln\left(\dfrac{C_{g1}}{C_{p1}} \right)}$. σ_1 and B_1 are phenomenological

membrane transport coefficients of reflection and permeation, respectively.

Transport of component 2 through the gel layer is

$$J_w C_{p2} = -\varepsilon_g D_2 \frac{dC_2}{dy} + J_w C_2 \tag{13.73}$$

where, C_{p2} and D_2 are the permeate concentration and diffusivity of component 2 and C_2 is the variable representing the concentration of component 2. ε_g is the gel

porosity and the compressibility effects are accounted using the functional form $\varepsilon_g = \varepsilon_0 (\Delta P)^{n_1}$. The above differential equation on integrating between the boundaries $y = [0, L]$ using the boundary condition, $C_2 = C_{gL2}$ at $y = L$leads to:

$$\frac{C_{gL2} - C_{p2}}{C_{gi2} - C_{P2}} = \exp\left(\frac{J_w L}{\varepsilon_g D_2}\right) \tag{13.74}$$

In the above equation, C_{gi2} and C_{gL2} are the concentration of component 2 at the gel-bulk and gel-membrane interface, respectively. Defining $v_1 = \dfrac{C_{gi2}}{C_{02}}$ and $v_2 = \dfrac{C_{gL2}}{C_{p2}}$, where, C_{02} as the feed concentration of component 2, Eq. (13.74) can be expressed as:

$$C_{p2} = \frac{v_1 C_{02} \exp\left(\dfrac{J_w L}{\varepsilon_g D_2}\right)}{v_2 - 1 + \exp\left(\dfrac{J_w L}{\varepsilon_g D_2}\right)} \tag{13.75}$$

The phenomenological equation to estimate the permeate flux is:

$$J_w = \frac{\Delta P}{\mu \left(R_m + R_g\right)} \tag{13.76}$$

In the above expression, μ is the solution viscosity, R_m is the membrane hydraulic resistance and R_g is resistance of the gel layer (Eq. 13.57). ρ_g is the gel layer density and the compressibility effect on specific cake resistance (α) is accounted as $\alpha = \alpha_0 (\Delta P)^{n_1}$. It may be noted the exponent (n_1) in the definition of α and ε is related to the effect of compressibility and considered to be the identical for both the parameters.

Thus, the problem reduces to the estimation of four variables J_w, C_{p1}, C_{p2} and L by solving the coupled Eqs. (13.70), (13.72), (13.75) and (13.75) simultaneously. The unknown parameters D_1, D_2 B_1, C_{g1}, ρ_g, σ_1, v_1, v_2, ε_0, α_0 and n_1 were determined by minimization of the sum of the residual function (S) represented by Eq. (13.77) using the experimental (superscript exp) and calculated (superscript cal) values. Optimization was carried out using twenty-seven experimental data points.

$$S = \Sigma\left(\frac{J_w^{cal} - J_w^{exp}}{J_w^{exp}}\right)^2 + \Sigma\left(\frac{C_{p1}^{cal} - C_{p1}^{exp}}{C_{p1}^{exp}}\right)^2 + \Sigma\left(\frac{C_{p2}^{cal} - C_{p2}^{exp}}{C_{p2}^{exp}}\right)^2 \tag{13.77}$$

Membranes with Low MWCO

In this model, component 2 cannot permeate freely through the membrane and its movement is hindered by both the membrane as well as the gel layer. Both component 1 and component 2 take part in the formation of gel layer. Therefore, the permeation of component 2 through the membrane also needs to be considered. Similar to the case of HMW solute, the expression for permeate flux and the permeation of component 1 through the membrane remains unaltered. In rearrangement of Eq. (13.74), v_2 is defined as $v_2 = \dfrac{C_{gL2}}{C_{mi2}}$, where C_{mi2} is the concentration of component 2 at the gel-membrane interface. Thus, Eq. (13.74) can be rearranged as

$$C_{p2} = \frac{v_2 C_{mi2} - v_1 C_{02} \exp\left(\dfrac{J_w L}{\varepsilon_g D_2}\right)}{1 - \exp\left(\dfrac{J_w L}{\varepsilon_g D_2}\right)} \tag{13.78}$$

The transport of component 2 through the membrane can be represented by modified Kedem-Katchalsky equation as:

$$J_w C_{P2} = B_2 \left(C_{mi2} - C_{pm02}\right) + \left(1 - \sigma_2\right)\overline{C_2} v_w \tag{13.79}$$

where, B_2 and σ_2 are the phenomenological membrane transport coefficients of permeation and reflection, respectively. C_{pm02} is the concentration of component 2 at the membrane-permeate interface on the membrane side. $\overline{C_2}$ is the logarithmic average concentration of component 2 defined as $\overline{C_2} = \dfrac{C_{mi2} - C_{pm02}}{\ln\left(\dfrac{C_{mi2}}{C_{pm02}}\right)}$ Eq. (13.79) can be rearranged as:

$$J_w C_{p2} = B_2 \left(C_{mi2} - v_3 C_{p2}\right) + \left(1 - \sigma_2\right)\overline{C_2} v_w \tag{13.80}$$

In the above equation, v_3 defined as $v_3 = \dfrac{C_{pm02}}{C_{p2}}$. Considering negligible mass transfer resistance between the membrane and the permeate side, $C_{pm02} \approx C_{p2}$ leading to the simplification $v_3 = 1$. Thus, the problem is reduced to determine the variables J_w, C_{p1}, C_{p2}, L and C_{mi2} by solving the coupled algebraic Eqs. (13.70), (13.72), (13.74), (13.78) and (13.80). Among the 13 unknown parameters (D_1, D_2, B_1, B_2, σ_1, σ_2, C_{g1}, ρ_g, v_1, v_2, v_3, α_0, ε_0 and n_1), the values of D_1, D_2, $\dfrac{C_{g1}}{C_{01}}$, $\dfrac{\rho_g}{\rho}$, v_1, ε_0, $\dfrac{\alpha_0}{R_m}$ and n_1 are intrinsic properties of the system and will remain identical as in case of the HMW case. This reduces the unknown parameters to be estimated as six, namely, B_1, B_2, σ_1, σ_2, v_2 and v_3. The solution methodology is similar to the HMW by minimizing the sum of residuals represented by Eq. (13.77).

The model as described above has been validated using experimental datasets with five different membranes, as presented in Table 13.3. Total dissolved solids

(TDS) is considered as component 1 and total polyphenols as component 2. Various parameters estimated using the model are presented in Table 13.3 for both high and low cut-off regimes. The non-zero value of n indicates compressible nature of the gel layer. The estimated values of gel layer thickness and permeate flux for high cut-off membranes are presented in Fig. 13.16, which indicates that the model predictions are within ±10% of the experimental results. The increase in gel layer thickness suggests continuous growth with TMP, which is higher in magnitude for GH membrane. Corresponding to this, the permeate flux also increases in the forward cycle due to increase in driving force but the effect of increased gel layer thickness is reflected as the diminishing slope. However, in reverse cycle, the permeate flux does not trace back the original path but exhibits lower values. This is due to the fact that the gel layer is not washed, and it keeps on accumulating offering increased resistance.

Similarly, the model predictions are also validated using experimental observations for low cut-off range and were observed to be within a relative error of ±10%. Theoretical results obtained have shown remarkable agreement of the gel layer thickness reported in literature. The additional variable in this case (C_{mi2}) was also estimated from the model and was found to be higher than the permeate concentration as expected. The variation in gel layer thickness was observed to be significantly less in reverse cycle as compared to the forward cycle for NFA and DK membranes. For the GE membrane, gel thickness increases with TMP up to 15 bar, beyond which it remains constant because of the counteracting flux of solute convection toward the membrane as well as solute permeation through the membrane. Thus, the permeate hysteresis is not observed

Table 13.3 Characteristics of membranes used in the experiments (Mondal et al. 2020)

Membrane type	GK	GH	GE	NFA-12A	DK
Membrane material	Polyamide-TFC				
Permeability (L/m².h.bar)	8.85	4.66	4.21	9.97	5.44
MWCO (Da)	3500	2500	1000	500	150–300
Operating pH range	2–10	2–10	2–10	3–11	3–9
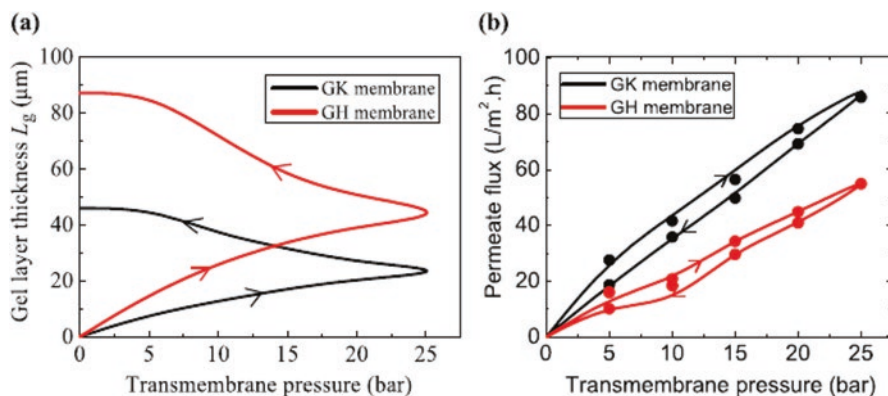
Fig. 13.16 For high MWCO membranes (a) variation in gel layer with TMP and (b) permeate flux as a function of TMP (symbols represent the experimental data points). (Reproduced from (Mondal et al. 2020) with permission from Elsevier Science and Technology Copyright 2020)

beyond 15 bar. At lower TMP, convective flux is less, and the gel thickness increases due to the deposition of solutes. It has been observed that the gel layer thickness is the maximum in case of GK membrane (87 μm) whereas for DK and NFA membranes, it is the lowest (5 μm). Thus, it may be concluded that membranes having higher MWCO exhibit thicker gel lay compared to low MWCO membranes. At all TMPs, the extraction of total phenols was observed to be the maximum for GK membrane.

3   Conclusions

The existing models for quantifying the performance of the membrane-based systems for processing of bioactive compounds were discussed in this chapter. The models were put under three broad classes as, empirical, semi-empirical and first principle-based models. The performance of the systems includes the prediction of permeate flux and permeate concentration. That indicates technical and economic feasibility, as well as the life of the membranes. The empirical models are basically black box type models assuming the permeate flux is represented by the driving force (TMP in this case) divided by several transport resistances in series (e.g., membrane resistance, fouling resistance, pore blocking resistance, etc.). The resistances were calculated from the experimental permeate flux data. One or more resistances were interrelated the dynamic permeate flux variations and the operating conditions (TMP and CFR). This resulted to the generation of the resistance in series models to predict the system performance at different operating conditions. Based on the consideration of membrane pore blocking during the filtration, two different variants of this model were discussed. The major advantages of empirical models are summarized as: (1) they provide easy and amenable method to model the system; (2) no in depth knowledge of the physico-chemical and transport properties of the solution and solvent are not needed; (3) no deeper knowledge of the mathematical or computational skill sets are required to use them; (4) the process operating parameters can be optimized easily and information about the limiting flux and corresponding operating conditions can be definitely determined. However, the limitations are: (1) these models can predict the permeate flux decline only, not the permeate concentration; (2) they are valid only within the studied range of the operating conditions and lose their predictive capability outside this range; (3) they lack the physical understanding of the involved transport process; (4) the results are system specific.

The semi-empirical models are one step ahead of the empirical models. In this case, the governing flux decline equations are based on the prevailing mechanisms and they are derived from the theoretical background. The original equations were obtained by Hermia and these models were modified by the continuous cross flow rate at steady-state (Field et al. 1995; Hermia 1982). The use of these models and their modified versions for sequential fouling mechanisms (like complete pore blocking followed by cake filtration) were demonstrated for quantification of flux decline of the solution containing bioactive compounds. The major advantage of

these models is that the underlying physical understanding behind the model equations is clear. The limitations of these models are: (1) they can predict only the permeate flux decline but cannot predict the history of permeate concentration; (2) the models fail when more than one mechanisms are in operation at a time; (3) since the model constants are evaluated for a particular solution and system, they are system specific and valid within the operating conditions studied.

The transport phenomena-based models are more versatile in nature. The underlying transport mechanisms provide strong foundation to formulate these models. In this case, the components of a complex plant extract / juice are clubbed in two groups, namely, larger sized components are grouped in higher molecular weight solutes that are mainly retained by the membrane forming a gel layer over the membrane surface. The lower molecular solutes are basically the desirable components (mostly the bioactive compounds) and the second component that is transported through the gel layer and the membrane reaching the permeate. Thus, the transport equations are written for various components in external mass transfer boundary layer, gel layer and membrane matrix. The equations are solved to get the system performance. The disadvantage of this model is that some of the transport coefficients of various components are unknown and they are obtained by using the experimental data. However, the advantages are many. These are (1) models are capable to predict the time history of permeate flux and permeate concentration; (2) the underlying physical principles are clear; (3) the model can be safely used for scaling up; (4) most importantly, they have the capability to predict the system performance at any operating conditions. Different variants of these models, for steady-state, transient under total recycle model, as well as the batch concentration mode, were presented in this chapter.

During a plant operation, it may not be possible to run the plant at constant TMP. Sometimes, TMP is increased to compensate the flux decline. Therefore, real time variation of steady state permeate flu with TMP is an important issue and it is termed as flux hysteresis. The modelling of hysteresis is therefore an important operating feature in actual plant operation and an a-priori knowledge would help the selection of the operating conditions and behavior of the flux history. The corresponding modelling of this complex phenomenon is also presented in this chapter. Demonstration of various modelling approaches in quantifying the performance of the membrane-based separation processes in case of filtration of bioactive compounds would be helpful to identify the flux decline mechanism, optimum operating conditions, system performance and definitely in designing and scaling up.

References

Aghdam MA, Mirsaeedghazi H, Aboonajmi M, Kianmehr MH (2015) Effect of ultrasound on different mechanisms of fouling during membrane clarification of pomegranate juice. Innov Food Sci Emerg Technol 30:127–131. https://doi.org/10.1016/j.ifset.2015.05.008

Agyei D, Danquah MK (2011) Industrial-scale manufacturing of pharmaceutical-grade bioactive peptides. Biotechnol Adv 29:272–277. https://doi.org/10.1016/j.biotechadv.2011.01.001

Bacchin P, Aimar P, Field RW (2006) Critical and sustainable fluxes: theory, experiments and applications. J Memb Sci 281:42–69

Blatt WF, Dravid A, Michaels AS, Nelsen L (1970) Solute polarization and cake formation in membrane ultrafiltration: causes, consequences and control techniques, in: membrane science and technology. Springer, New York, pp 47–97

Bowen WR, Calvo JI, Hernández A (1995) Steps of membrane blocking in flux decline during protein microfiltration. J Memb Sci 101:153–165. https://doi.org/10.1016/0376-7388(94)00295-A

Bungay PM, Lonsdale HK, Pinho MN (1983) Synthetic membranes: science, engineering and applications, NATO ASI series. Reidel, Boston, p 181

Cancino-Madariaga B, Ruby R, Astudillo Castro C, Saavedra Torrico J, Lutz Riquelme M (2012) Analysis of the membrane fouling mechanisms involved in clarified grape juice ultrafiltration using statistical tools. Ind Eng Chem Res 51:4017–4024. https://doi.org/10.1021/ie201921x

Cassano A, Marchio M, Drioli E (2007) Clarification of blood orange juice by ultrafiltration: analyses of operating parameters, membrane fouling and juice quality. Desalination 212:15–27

Conidi C, Cassano A, Drioli E (2012) Recovery of phenolic compounds from orange press liquor by nanofiltration. Food Bioprod Process 90:867–874. https://doi.org/10.1016/j.fbp.2012.07.005

Das A, Paul D, Golder AK, Das C (2015) Separation of Rebaudioside-A from stevia extract: membrane selection, assessment of permeate quality and fouling behavior in laminar flow regime. Sep Purif Technol 144:8–15. https://doi.org/10.1016/j.seppur.2015.02.004

De Barros STD, Andrade CMG, Mendes ES, Peres L (2003) Study of fouling mechanism in pineapple juice clarification by ultrafiltration. J Memb Sci 215:213–224

De S, Bhattacharya PK (1997) Modeling of ultrafiltration process for a two-component aqueous solution of low and high (gel-forming) molecular weight solutes. J Memb Sci 136:57–69. https://doi.org/10.1016/S0376-7388(97)00177-4

De S, Dias JM, Bhattacharya PK (1997) Short and long term flux decline analysis in ultrafiltration. Chem Eng Commun 159:67–89. https://doi.org/10.1080/00986449708936594

dos Santos Sousa L, Cabral BV, Madrona GS, Cardoso VL, Reis MHM (2016) Purification of polyphenols from green tea leaves by ultrasound assisted ultrafiltration process. Sep Purif Technol 168:188–198. https://doi.org/10.1016/j.seppur.2016.05.029

Field RW, Pearce GK (2011) Critical, sustainable and threshold fluxes for membrane filtration with water industry applications. Adv Colloid Interf Sci 164:38–44

Field RW, Wu D, Howell JA, Gupta BB (1995) Critical flux concept for microfiltration fouling. J Memb Sci 100:259–272. https://doi.org/10.1016/0376-7388(94)00265-Z

Firdaous L, Dhulster P, Amiot J, Gaudreau A, Lecouturier D, Kapel R, Lutin F, Vézina LP, Bazinet L (2009) Concentration and selective separation of bioactive peptides from an alfalfa white protein hydrolysate by electrodialysis with ultrafiltration membranes. J Memb Sci 329:60–67. https://doi.org/10.1016/j.memsci.2008.12.012

Galanakis CM (2015) Separation of functional macromolecules and micromolecules: from ultrafiltration to the border of nanofiltration. Trends Food Sci Technol 42:44–63. https://doi.org/10.1016/j.tifs.2014.11.005

Gekas V, Hallström B (1987) Mass transfer in the membrane concentration polarization layer under turbulent cross flow: I. critical literature review and adaptation of existing sherwood correlations to membrane operations. J. Memb Sci 30:153–170. https://doi.org/10.1016/S0376-7388(00)81349-6

Gerke IBB, Hamerski F, Scheer AP, Silva VR (2017) Clarification of crude extract of yerba mate (Ilex paraguariensis) by membrane processes: analysis of fouling and loss of bioactive compounds. Food Bioprod Process 102:204–212. https://doi.org/10.1016/j.fbp.2016.12.008

Giacobbo A, Bernardes AM, de Pinho MN (2017) Sequential pressure-driven membrane operations to recover and fractionate polyphenols and polysaccharides from second racking wine lees. Sep Purif Technol 173:49–54. https://doi.org/10.1016/j.seppur.2016.09.007

Guo W, Ngo HH, Li J (2012) A mini-review on membrane fouling. Bioresour Technol 122:27–34. https://doi.org/10.1016/j.biortech.2012.04.089

Hermia J (1982) Constant pressure blocking filtration laws-application to power law non-Newtonian fluids. Trans IChmE 60:183–187

Ho C, Zydney AL (2000) A combined pore blockage and cake filtration model for protein fouling during microfiltration. J Colloid Interface Sci 232:389–399. https://doi.org/10.1006/jcis.2000.7231

Ilame SA, Satyavir VS (2015) Application of membrane separation in fruit and vegetable juice processing: a review. Crit Rev Food Sci Nutr 55:964–987. https://doi.org/10.1080/10408398.2012.679979

Jaffrin MY (2012) Hydrodynamic techniques to enhance membrane filtration. Annu Rev Fluid Mech 44:77–96

Jain A, Sengupta S, De S (2018) Fundamental understanding of fouling mechanisms during microfiltration of bitter gourd (Momordica charantia) extract and their dependence on operating conditions. Food Bioprocess Technol 11:1012–1026

Jian P, Yahui HE, Yang W, Linlin L (2006) Preparation of polysulfone--Fe3O4 composite ultrafiltration membrane and its behavior in magnetic field. J Memb Sci 284:9–16

Johnston ST, Deen WM (2002) Hindered convection of ficoll and proteins in agarose gels. Ind Eng Chem Res 41:340–346. https://doi.org/10.1021/ie010085s

Katzir-Katchalsky A, Curran PF (1965) Nonequilibrium thermodynamics in biophysics. Harvard University Press, Cambridge, MA, pp 113–180

Kumar A, Thakur BK, De S (2012) Selective extraction of (−)epigallocatechin Gallate from green tea leaves using two-stage infusion coupled with membrane separation. Food Bioprocess Technol 5:2568–2577. https://doi.org/10.1007/s11947-011-0580-0

Kurada KV, De S (2018) Polyaniline doped ultrafiltration membranes: mechanism of membrane formation and pH response characteristics. Polymer (Guildf) 153:201–213. https://doi.org/10.1016/j.polymer.2018.08.032

Ma H, Bowman CN, Davis RH (2000) Membrane fouling reduction by backpulsing and surface modification. J Memb Sci 173:191–200. https://doi.org/10.1016/S0376-7388(00)00360-4

Mondal S, De S (2009) Generalized criteria for identification of fouling mechanism under steady state membrane filtration. J Memb Sci 344:6–13. https://doi.org/10.1016/j.memsci.2009.08.015

Mondal S, De S (2010) A fouling model for steady state crossflow membrane filtration considering sequential intermediate pore blocking and cake formation. Sep Purif Technol 75:222–228. https://doi.org/10.1016/j.seppur.2010.07.016

Mondal M, De S (2018) Enrichment of (−) epigallocatechin gallate (EGCG) from aqueous extract of green tea leaves by hollow fiber microfiltration: modeling of flux decline and identification of optimum operating conditions. Sep Purif Technol 206:107–117. https://doi.org/10.1016/j.seppur.2018.05.057

Mondal M, De S (2019) Purification of polyphenols from green tea leaves and performance prediction using the blend hollow fiber ultrafiltration membrane. Food Bioprocess Technol:933–953. https://doi.org/10.1007/s11947-019-02262-6

Mondal S, Cassano A, Tasselli F, De S (2011) A generalized model for clarification of fruit juice during ultrafiltration under total recycle and batch mode. J Memb Sci 366:295–303. https://doi.org/10.1016/j.memsci.2010.10.015

Mondal S, Chhaya D, De S (2012a) Prediction of ultrafiltration performance during clarification of stevia extract. J Memb Sci 396:138–148. https://doi.org/10.1016/j.memsci.2012.01.009

Mondal S, Chhaya, De S (2012b) Modeling of cross flow ultrafiltration of stevia extract in a rectangular cell. J Food Eng 112:326–337. https://doi.org/10.1016/j.jfoodeng.2012.05.002

Mondal S, Rai C, De S (2013) Identification of fouling mechanism during ultrafiltration of stevia extract. Food Bioprocess Technol 6:931–940. https://doi.org/10.1007/s11947-011-0754-9

Mondal S, Egea-Corbacho A, Conidi C, Cassano A, De S (2020) Permeate flux hysteresis with transmembrane pressure in the gel controlling membrane filtration. J Food Eng 264:109689. https://doi.org/10.1016/j.jfoodeng.2019.109689

Mukherjee R, De S (2016) Novel carbon-nanoparticle polysulfone hollow fiber mixed matrix ultrafiltration membrane: adsorptive removal of benzene, phenol and toluene from aqueous solution. Sep Purif Technol 157:229–240. https://doi.org/10.1016/j.seppur.2015.11.015

Pabby AK, Rizvi SSH, Sastre AM (2015) Handbook of membrane separations: chemical, pharmaceutical, food, and biotechnological applications, 2nd edn. Taylor and Francis Group\CRC Press, Boca Raton. https://doi.org/10.1201/b18319

Padaki M, Murali RS, Abdullah MS, Misdan N, Moslehyani A, Kassim MA, Hilal N, Ismail AF (2015) Membrane technology enhancement in oil – water separation: a review. Desalination 357:197–207

Poulin JF, Amiot J, Bazinet L (2006) Simultaneous separation of acid and basic bioactive peptides by electrodialysis with ultrafiltration membrane. J Biotechnol 123:314–328. https://doi.org/10.1016/j.jbiotec.2005.11.016

Rai P, Majumdar GC, Sharma G, Das Gupta S, De S (2006) Effect of various cutoff membranes on permeate flux and quality during filtration of Mosambi (Citrus sinensis (L.) Osbeck) juice. Food Bioprod Process 84:213–219. https://doi.org/10.1205/fbp.05181

Rai C, Rai P, Majumdar GC, De S, DasGupta S (2010) Mechanism of permeate flux decline during microfiltration of watermelon (Citrullus lanatus) juice. Food Bioprocess Technol 3:545–553. https://doi.org/10.1007/s11947-008-0118-2

Reis MHM, Da Silva FV, Andrade CMG, Rezende SL, Wolf MacIel MR, Bergamasco R (2009) Clarification and purification of aqueous stevia extract using membrane separation process. J Food Process Eng 32:338–354. https://doi.org/10.1111/j.1745-4530.2007.00219.x

Roy A, De S (2014) Extraction of steviol glycosides using novel cellulose acetate pthalate (CAP) – Polyacrylonitrile blend membranes. J Food Eng 126:7–16. https://doi.org/10.1016/j.jfoodeng.2013.10.035

Roy A, De S (2015) Resistance-in-series model for flux decline and optimal conditions of stevia extract during ultrafiltration using novel CAP-PAN blend membranes. Food Bioprod Process 94:489–499. https://doi.org/10.1016/j.fbp.2014.07.006

Skinner M, Hunter D (2013) Bioactives in fruit: health benefits and functional foods. Wiley, Oxford

Song YQ, Sheng J, Wei M, Yuan XB (2000) Surface modification of polysulfone membranes by low-temperature plasma-graft poly(ethylene glycol) onto polysulfone membranes. J Appl Polym Sci 78:979–985. https://doi.org/10.1002/1097-4628(20001031)78:5<979::AID-APP60>3.0.CO;2-U

Tasselli F, Cassano A, Drioli E (2007) Ultrafiltration of kiwifruit juice using modified poly(ether ether ketone) hollow fibre membranes. Sep Purif Technol 57:94–102. https://doi.org/10.1016/j.seppur.2007.03.007

Trettin DR, Doshi MR (1980) Ultrafiltration in an unstirred batch cell. Ind Eng Chem Fundam 19:189–194

Vladisavljević GT, Vukosavljević P, Bukvić B (2003) Permeate flux and fouling resistance in ultrafiltration of depectinized apple juice using ceramic membranes. J Food Eng 60:241–247. https://doi.org/10.1016/S0260-8774(03)00044-X

Wandera D, Wickramasinghe SR, Husson SM (2010) Stimuli-responsive membranes. J Memb Sci 357:6–35